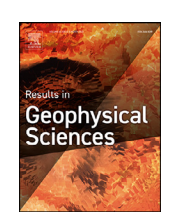
ELSEVIER

Contents lists available at ScienceDirect

# **Results in Geophysical Sciences**

journal homepage: www.elsevier.com/locate/ringps



# Reconstructing the depositional history and age of fossil-bearing palaeokarst: A multidisciplinary example from the terminal Pliocene Aves Cave Complex, Bolt's farm, South Africa



Tara R. Edwards a,b,c,1,\*, Robyn Pickering b,c, Tom L. Mallett a, Andy I.R. Herries a,d

- <sup>a</sup> The Australian Archaeomagnetism Laboratory, Department of Archaeology and History, La Trobe University, Bundoora 3086, VIC, Australia
- <sup>b</sup> Department of Geological Science, University of Cape Town, Rondebosch 7700, Western Cape, South Africa
- <sup>c</sup> Human Evolution Research Institute, University of Cape Town, Rondebosch 7700, Western Cape, South Africa
- <sup>d</sup> Palaeo-Research Institute, University of Johannesburg, Auckland Park 2092, Gauteng, South Africa

### ARTICLE INFO

# Keywords: Palaeocave Geochronology Palaeomagnetism Sedimentology Palaeontology South Africa

# ABSTRACT

The region ~40 km north-west of Johannesburg, South Africa, known locally as the Cradle of Humankind, is of global significance as the caves preserve Plio-Pleistocene faunal and early hominin fossils. Despite a long history of research, there is still a need to contextualise and date the remarkable collection of fossils. An important but understudied palaeontological site, Bolt's Farm, may provide a key to addressing this as it preserves a series of >20 separate eroded palaeocave remnants occurring across a 1 km length of hillside. This is in contrast to highly concentrated deposits representing a single site, as is the case at the majority of the sites in the region. Historically, a lithostratigraphic approach to South African palaeocaves made reconstruction and comparison within, and between, deposits difficult or impossible. Here, we present a sequence stratigraphic approach and simple facies model for three palaeocave remnants at Bolt's Farm collectively termed the Aves Cave Complex (ACC), and a chronology based on combined uranium lead (U-Pb) dating, of basal and capping flowstones, and palaeomagnetic analysis. Results indicate that these currently discrete localities, formed together from a single entry dating to the end of the Gauss Normal Polarity Chron between 3.03 and 2.61 Ma, making ACC one of the oldest directly dated fossil deposits in the Cradle. The ACC contains the earliest occurrence of a key biochronological species. Metridiochoerus andrewsi, in the region. This work reinforces the model that clastic sedimentation and flowstone precipitation do not occur concurrently in Cradle caves; rather their mutually exclusive formation is driven by allocyclic changes in hydroclimate. This research contributes to understanding how Bolt's Farm developed the unprecedented high density of palaeokarst observed today, by offering the first evidence that currently discrete localities were once connected as a single cave system.

# 1. Introduction

The Cradle of Humankind (Cradle) comprises a number of palaeokarst deposits preserving the earliest hominin fossils and archaeology in South Africa (Fig. 1; Herries et al., 2013, Wood and Boyle 2016, Stammers et al., 2018; Herries et al., 2020). Formed within the ~2.50 Ga Malmani Subgroup of the Transvaal Supergroup, the karst system is a complex series of active caves (e.g. Sterkfontein Caves, Wonder Cave) and remnant palaeokarst with bone bearing clastic deposits (e.g. Malapa, Kromdraai, Swartkrans). These sites occur in an area of 150 km² about 40 km north-west of Johannesburg in Gauteng Province and have been the subject of research for decades (Broom 1936; 1938; Broom and

Robinson 1949; Susman 1988; 1989; Brain 1993; De Ruiter and Berger 2000; Keyser et al., 2000; Berger et al., 2010; 2015). Two satellite sites, the Makapansgat Limeworks (MKP), ~250 km to the north-east in Limpopo Province and the Buxton-Norlim Limeworks near Taung in North West Province, about 350 km to the south-west, also contain important early hominin (*Australopithecus africanus*) fossils (Fig. 1; Dart, 1925; 1955, Herries et al., 2013).

Research in the Cradle has primarily focused on the discovery of fossil remains of early hominin species (e.g. *A. africanus, Paranthropus robustus, Homo* aff. *erectus*,) and other mammals (Dart 1925; Broom 1939; Freedman 1957; Cooke 1993; Clarke 1998; Berger et al., 2002; Partridge et al., 2003; Gommery et al., 2008a; Herries et al., 2020).

<sup>\*</sup> Corresponding author at: The Australian Archaeomagnetism Laboratory, Department of Archaeology and History, La Trobe University, Bundoora 3086, VIC, Australia.

E-mail address: Tara.Edwards@uct.ac.za (T.R. Edwards).

<sup>1</sup> Present address: Department of Geological Science, University of Cape Town, Rondebosch 7700, Western Cape, South Africa.

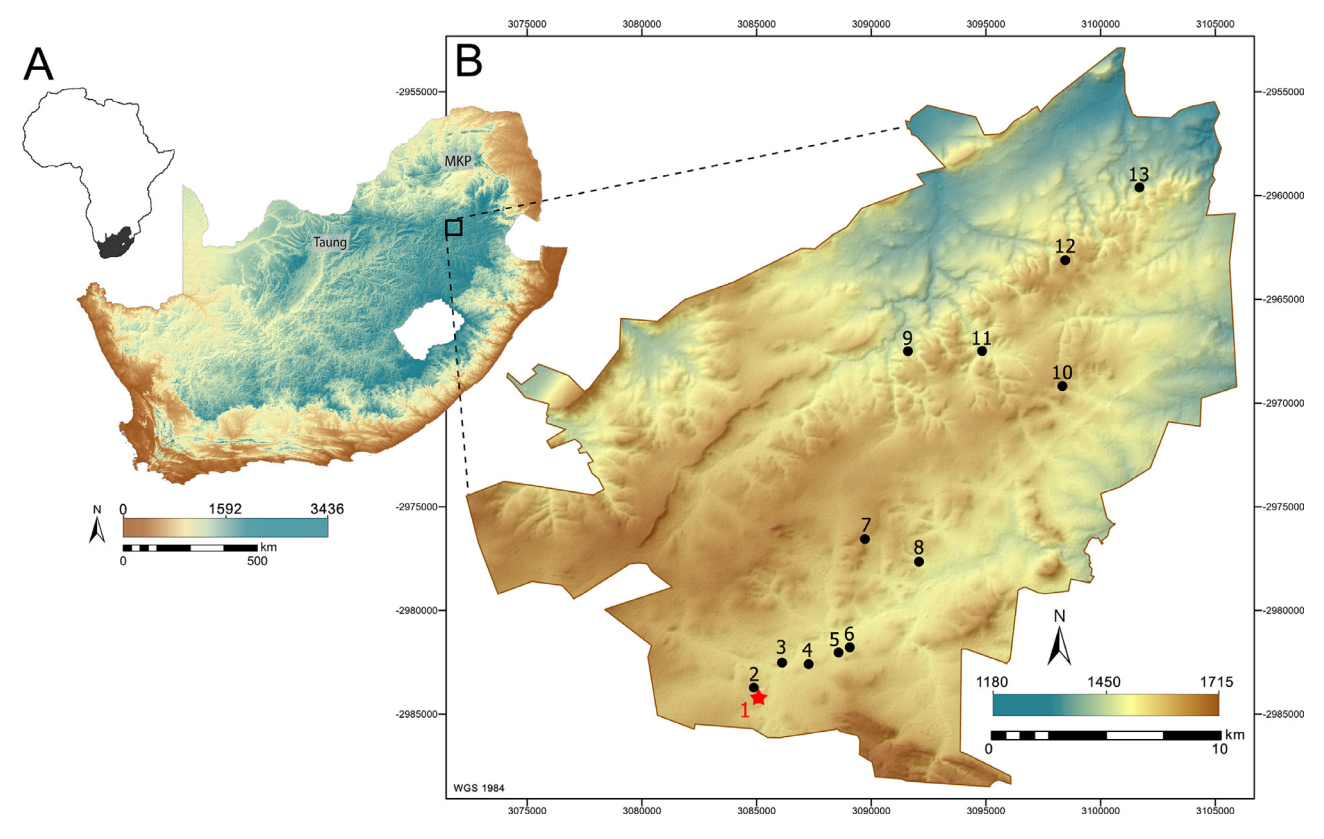


Fig. 1. A) Map of South Africa showing location of the Cradle and two satellite sites of Makapansgat Limeworks (MKP) and Taung. B) Inset showing the key fossil bearing sites in the Cradle: 1) Bolt's Farm 2) Rising Star 3)Swartkrans 4) Sterkfontein 5) Cooper's 6) Kromdraai 7) Drimolen 8) Plover's Lake 9) Gladysvale 10) Malapa 11) Motsetse 12) Haasgat and 13) Gondolin. Elevation data made available from Jarvis et al. 2008, figure adapted from Edwards et al. (2019).

Broad climatic conditions, such as vegetation type (C3/C4) and rainfall can be gained through the analysis of stable isotopes from fossil teeth, as well as cave deposits (Van der merwe and Thackeray 1997; Sponheimer et al., 1999; Lee Thorp et al. 2000; Hopley et al., 2007; Pickering et al., 2007). While there was an early interest in the geological and sedimentological context of fossil sites (Cooke 1938; Haughton 1947; King 1951; Brain 1958; Wilkinson 1973; 1983), there was a transition towards simple 'layer cake' stratigraphies, with lithostratigraphic interpretations produced for many sites (Partridge 1978; 2000). This saw the classification of lithologically distinct clastic units or 'Members' developed for sites such as Swartkrans, Sterkfontein and the Makapansgat Limeworks (Brain 1976; Butzer 1976; Partridge 1978; 1979; 2000). Numbering of these Members was used to infer a chronology for the clastic deposits. However, due to the nature of depositional processes within a cave, units which are lithologically similar may be chronologically disparate.

The lithostratigraphic approach of the Member system left a gap in investigating the three-dimensional sedimentary architecture of the deposits and subsequent understanding of the lateral distribution of depositional environments as a function of the life history of the cave. This, combined with the perceived lack of 'dateable' deposits, compared with eastern Africa, hampered the development of robust geochronologies for Cradle sites. However, clastic fossil bearing sediments are not the only type of deposits preserved in the Cradle caves. Speleothems are ubiquitous features and consist of rare stalagmites, stalactites and most commonly laterally extensive horizontally bedded layers of calcium carbonate termed flowstones. Although the bulk of speleothem deposits were heavily mined, flowstones are present at every site, found either between the basal contact of the host rock and clastic sediments, and/or interbedded between the fossil bearing sediments (Pickering et al., 2019). External variation in hydroclimate, from wet to dry to wet, is the likely mechanism responsible for such sequence of flowstone to clastic sediment and flowstone again (Ayliffe et al., 1998, Moriarty et al. 2000, Lacruz et al., 2002, Pickering et al., 2007; 2019). The layer of clastic sediment sandwiched between a basal and capping flowstone is termed a 'Flowstone Bounded Unit' (FBU) (Moriarty et al. 2000; Pickering et al., 2007). Given the basic principle of hydrodynamic sorting, clastic sediment accumulated at the entrance of a cave will be coarser grained than the distal equivalent deposits; however, if these two sediments are bound by the same flowstone, they can be grouped as a FBU. This chronostratigraphic approach, using the flowstones to divide the sediments up into units, avoids the issues of lithostratigraphy by recognizing that flowstones form in discrete periods and subsequently act as sedimentary timelines (Pickering et al., 2007).

The last decade has seen the proliferation of site specific dating (Herries et al., 2006; 2014; Herries et al., 2020; Pickering et al., 2007; Berger et al., 2010; Pickering et al., 2010; Herries and Shaw 2011; Granger et al., 2015; Dirks et al., 2017) and landscape evolution studies (Dirks and Berger 2013), with a recent regional study suggesting that the dynamics of deposition within Cradle caves is driven by variation in hydroclimate (Pickering et al., 2019). Under this model, precipitation of speleothems occurs during specific windows named 'Flowstone Growth Intervals' (FGIs). Between 3.2–1.3 Ma Pickering et al. (2019) identified 6 FGIs from eight Cradle sites.

The intervening periods are classified as times of sediment accumulation (SED 1–6). It is during the SED periods that clastic and fossil-bearing units would have been deposited within the Cradle caves (Pickering et al., 2019). However, continued site-specific studies are necessary to improve our understanding of local conditions and cave specific controls on deposition. Bolt's Farm is of particular interest as it differs from many sites in the Cradle, preserving a high density (>20) of discrete, heavily eroded palaeokarst localities (Fig. 2). However, how these currently discrete localities relate to one another remains an open question: were they small, discrete caves or were they connected as a

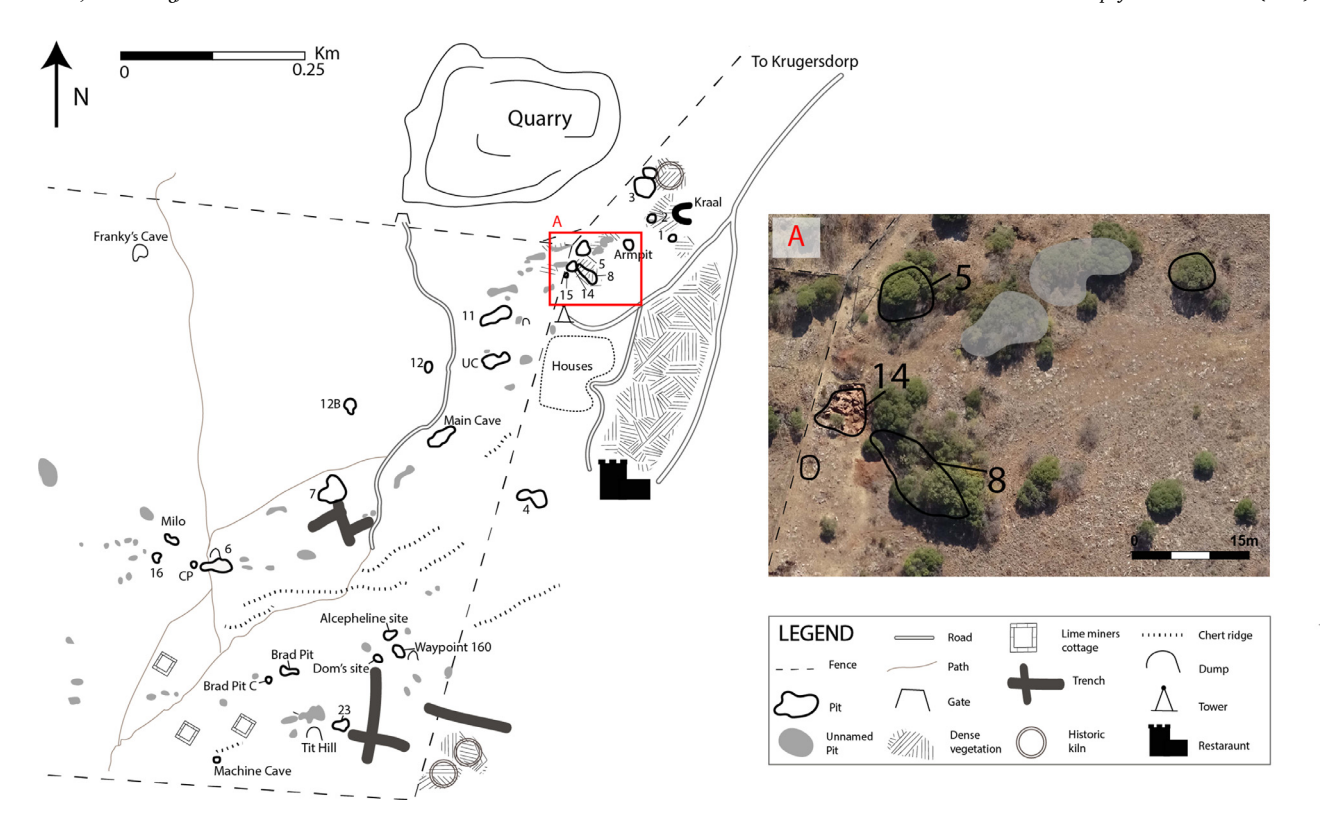


Fig. 2. Map of Bolt's Farm localities with inset A) showing aerial imagery of the proposed Aves Cave Complex consisting of Pits 14, 5 and 8. Figure adapted from Edwards et al. (2019).

part of a larger cave system? At some local sites, like Drimolen, dating has shown that the Drimolen Makondo (DMK) and Drimolen Main Quarry (DMQ) deposits that are only 50 m from each other are of distinctly different ages, 2.61 Ma at DMK and 2.04–1.95 Ma at DMQ (Herries et al., 2018; Herries et al., 2020). At Kromdraai, the archaeology bearing Kromdraai A (KA) was originally considered to be a separate deposit from the 30 m distant hominin bearing Kromdraai B (KB) deposits based on apparent temporal differences, but recent research suggests that deposits seen at KA are also seen at KB (Braga et al., 2017).

Today Bolt's Farm consists of a series of active caves and palaeokarst remnants split across three properties (Fig. 2). The northern extent consists of a large quarry where fossil bearing deposits identified in the 1940s have since been excavated away (Edwards et al., 2019). The majority of palaeokarst deposits and caves are centred on a 1 km<sup>2</sup> property (Klinkert's) and several more are preserved along the eastern portion (Greensleeves). Like most sites in the Cradle, the Bolt's Farm deposits were extensively mined for speleothem in the late 19th and early 20th century (Edwards et al., 2019), although the history of mining is not well documented. Palaeontological interest at Bolt's Farm began with Robert Broom's 1936 exploration of caves in the region (Broom 1937, 1939). However, with the discovery of Australopithecus at Sterkfontein that same year (Broom 1936; 1939) more extensive survey work and fossil collection at Bolt's Farm did not take place until 1948 by the University of California Africa Expedition (UCAE; Monson et al., 2015, Edwards et al., 2019).

Studies of this faunal material by Cooke (1991) showed the importance of Bolt's Farm for understanding the evolution of a number of taxa that have been used as key biochronological markers in South Africa, particularly Stage I *Metridiochoerus andrewsi* and *Dinofelis barlowi*. Staggered research has been conducted at the site since the 1990s, with a focus on unearthing many of the palaeocaves, as well as excavating faunal remains (Pickford and Gommery 2016). This work led to the recovery of more *in-situ* material from sites identified by the UCAE, as well as from

new localities (e.g. Waypoint 160; Sénégas and Avery 1998). Initially, there was considerable confusion with regards to which deposits were which, however recent work has helped to resolve this, with new aerial and ground surveys of the site and comparisons to UCAE surveys from the 1940s (Edwards et al., 2019).

The various fossil sites across the surface of Bolt's Farm have often been referred to as lime miners 'pits' and may represent excavation into single, small palaeocave deposits, or in other cases, excavations into different parts of the same large, palaeocave infill. Due to this anthropogenic alteration and the fact that many fossil sites are merely shallow, heavily eroded remnants, it has been difficult to reconstruct what the caves originally looked like and whether separate 'pits' or palaeocave exposures represent the same or multiple deposits. There does appear to be some temporal difference between pits across the whole of Bolt's Farm with some containing fossils of Equus, suggesting and age of <2.3 Ma, and others containing species that may suggest an older Pliocene age (Edwards et al., 2019). However, because there are so few Pliocene (and > 2 Ma old) sites in South Africa, compared to sites between ~2 Ma and 1.3 Ma, the nature of change in species such Metridiochoerus andrewsi (Stage I at the 3.0-2.6 Ma Makapansgat Limeworks and Stage III at the ~1.8 Ma Gondolin site) is still not well understood in the region. Working to resolve this will better inform site reconstruction on a landscape scale. This study is the first to use stratigraphic observation, combined U-Pb dating and palaeomagnetism to reconstruct the depositional history of three currently discrete 'pits' to test the hypothesis that they were part of a larger cave system.

# 2. Bolt's farm geological setting

The regional host rock, the Malmani Subgroup of the Transvaal Supergroup, was originally laid down as a carbonate platform in the Palaeoproterozoic era (~2.60–2.40 Ga) within an epeiric sea, which existed across a large portion of the ancient Kaapvaal Craton (Button 1973,

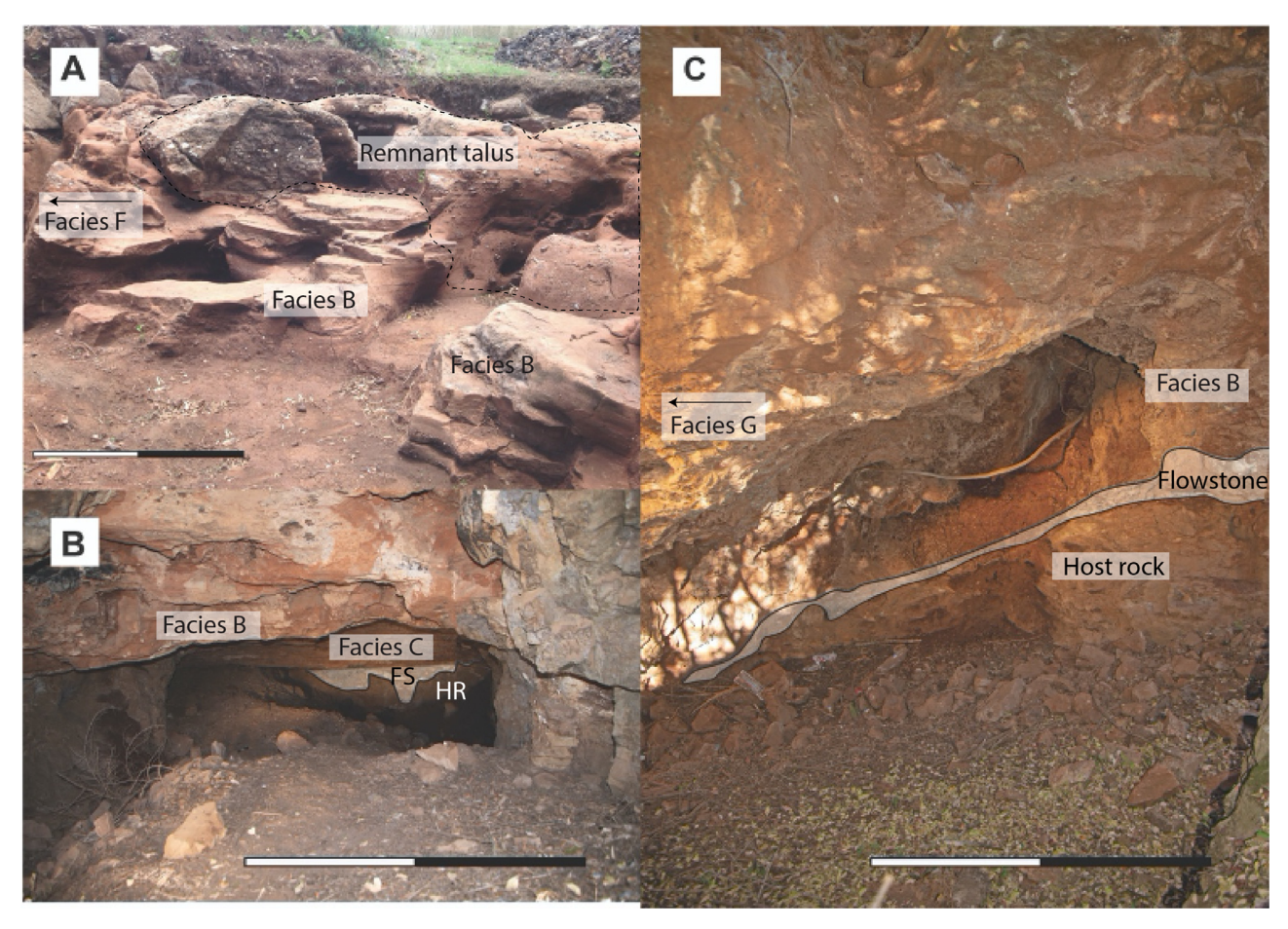


Fig. 3. Site photos for the three pits comprising the Aves Cave Complex, scale bars represent 1 m. A) Pit 14 is composed of coarse talus deposits as well as fine deposits. Photo facing NW. B) Pit 5 is composed of winnowed deposits. Basal flowstone highlighted. Photo facing W.C) Sediments at Pit 8 are preserved along a single wall. Basal flowstone highlighted. Photo facing W.

Eriksson and Truswell 1975, Eriksson et al., 1993, Obbes 2000). There are five formations within the Malmani Subgroup; Oaktree, Monte Christo, Lyttelton, Eccles and Frisco, defined primarily on the basis of stromatolite type and chert content (Button 1973, Eriksson and Truswell 1975, SACS 1979, SACS 1980, Obbes 2000, Ingram and van Tonder 2011). To date, no published studies have focused on which formation Bolt's Farm sits within, however, the nearby site of Sterkfontein straddles the boundary of the Oaktree and Monte Christo (Martini et al., 2003).

The landscape at Bolt's Farm represents a heavily eroded surface, pitted with remnants of caves and stratigraphically isolated fossil bearing palaeokarst deposits (Fig. 2). The terms 'palaeocaves' and 'palaeokarst' refer to an ancient de-roofed cave with mostly indurated sediments and the ancient karst landscape in which these caves have formed, respectively. Of interest here are three currently discrete localities within close proximity: Pit 14, Pit 5 and Pit 8 (Fig. 2A).

Pit 14, originally named Benchmark Pit due to its proximity to the benchmark set up for mapping in 1948, has subsequently become known as Aves Cave (1) (Pickford and Gommery 2016; Edwards et al., 2019) and consists of a palaeokarst remnant with preserved outcrops of clastic sedimentary rocks (sandstone, siltstone, 'cave breccia') and speleothem (Fig. 3). Pit 14 was identified and collected from by the UCAE in 1948 and presents some of the most biochronologically significant faunal material in this area, of particular and continuing interest was the recovery of several specimens attributed to Stage I Metridiochoerus andrewsi (also defined as Potamochoeroides shawi or Potamochoeroides hypsodont;

Pickford and Gommery, 2016) similar to that from Makapansgat Limeworks estimated to date to between to 3.03 and 2.61 Ma (Herries et al., 2013; Pickford and Gommery 2016; Edwards et al., 2019). Pit 5 is a small, roofed cavern (5×7 m), located ~15 m north-east of Pit 14 with exposed stratigraphy along the western and northern walls and ceiling. Lithologies include siltstones, sandstones and flowstones (Fig. 3B), with no biochronologically informative species known from the deposits (Edwards et al., 2019). Pit 8 is located immediately to the south east of Pit 14 (Fig. 2A, Fig. 3C). Lithified sediments preserved at this location include flowstone, siltstone and sandstone, along with large chert blocks (<1.5 m) representing ceiling collapse. Plentiful rodent fossils and few large mammals (bovid and felid) have been recovered from Pit 8 (Gommery et al., 2016). Due to the limited palaeontological remains, there has been little investigation of Pits 5 and 8 and up until now how they relate to Pit 14 has not been investigated.

# 3. Materials & methods

# 3.1. Fieldwork: survey and mapping methods

High resolution aerial imagery was previously collected using an eBee senseFly drone, with all details of data collection and processing detailed in Edwards et al. (2019). Similarly, a feature-based foot survey of Bolt's Farm (Klinkert's and Greensleeves) was carried out using a Leica GPS1200+ Differential Global Positioning System (DGPS). This allowed for sub-centimetre accuracy of all surveyed positions, includ-

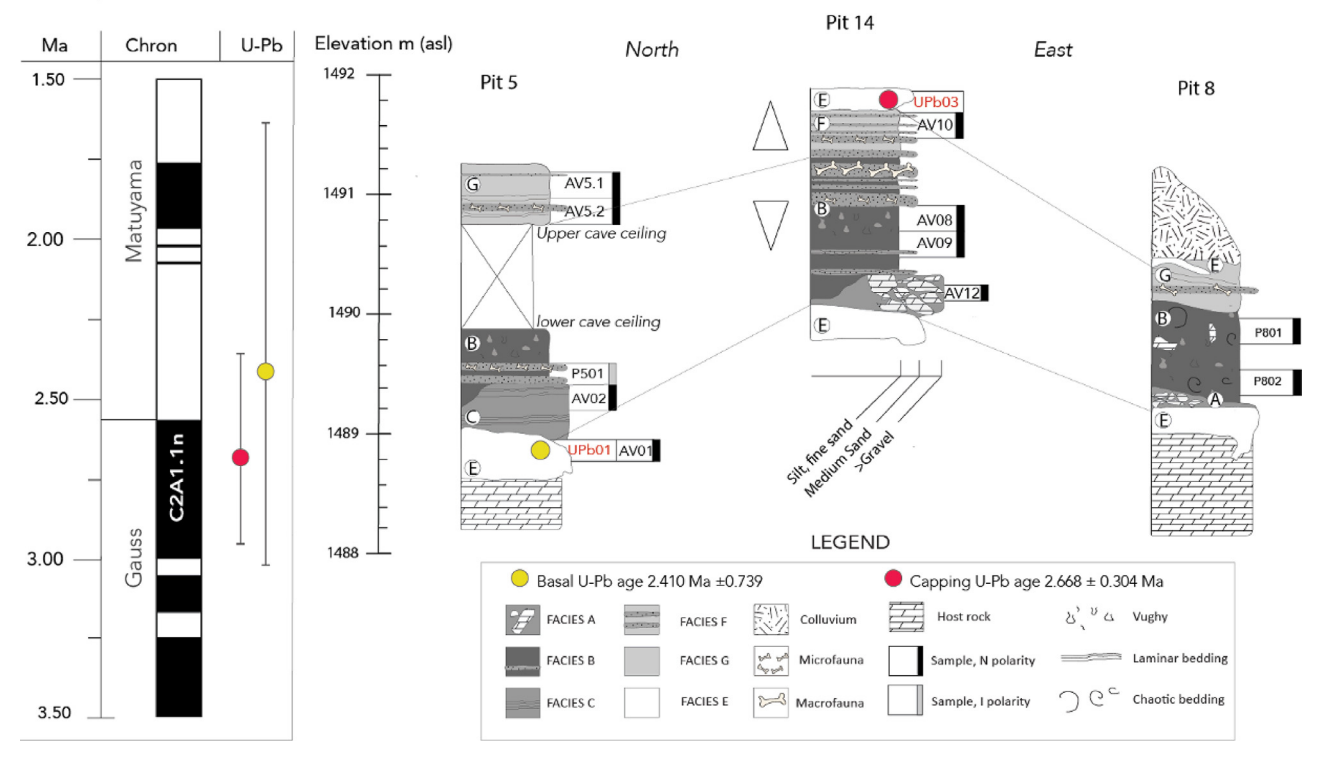


Fig. 4. Composite magnetostratigraphy and facies for the Aves Cave Complex (Pits 14, 5 and 8) at Bolt's Farm.

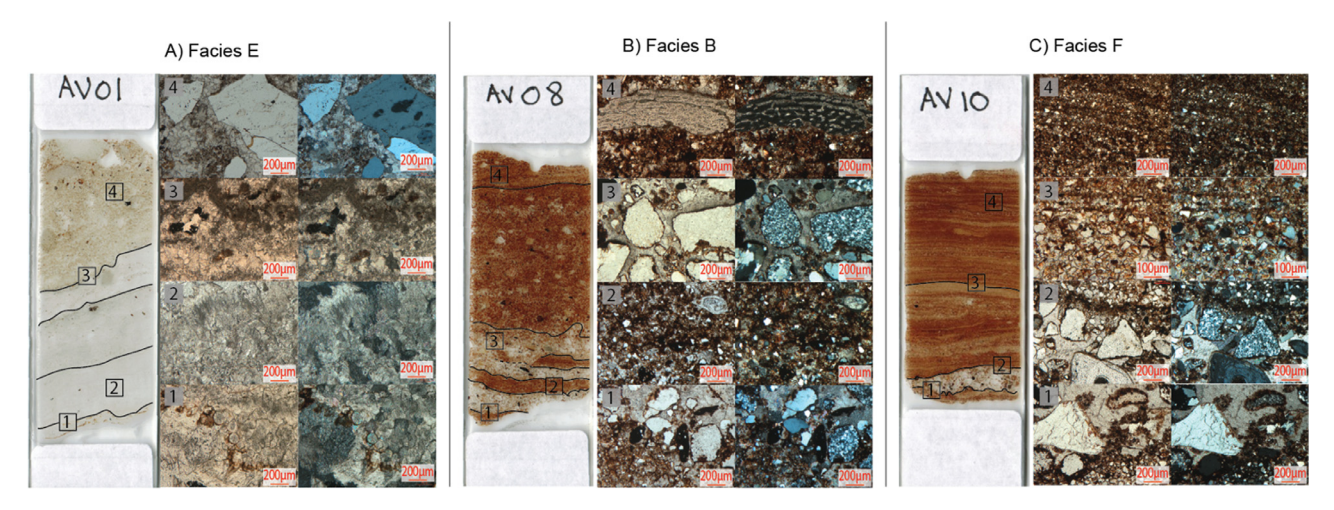


Fig. 5. Thin section and photomicrographs for the ACC. A) Sample AV01 represents the basal flowstone from Pit 5 and Facies E B) Sample AV08 exhibits the vuggy nature of Facies B from Pit 14. C) Sample AV10 represented Facies F and shows a fining up sequence of laminated silt and sand.

ing location of Pits 14, 5, 8. Full details of DGPS data collection and processing are given in Edwards et al. (2019).

# 3.2. Stratigraphic methods, thin section preparation and analysis

Stratigraphic sections (and samples) were taken in locations with the most complete sediment outcrop. Following Lacruz et al. (2002) and Pickering et al. (2007) a sequence stratigraphic approach was applied to the deposits of Pits 14, 5 and 8, where the presence of flowstone marks a temporal hiatus in the accumulation of sediment. Subsequently, a facies model was developed which separated stratigraphic units on the basis of colour, textural composition, fossil content, bedding and sedimentary structures. Stratigraphic logs for the three pits can be seen in Fig. 4.

Thin sections were prepared to assist with lithofacies identification (Fig. 5). An additional aim of the petrographic analysis was to deter-

mine mode of deposition and assess the viability of samples for palaeomagnetic analysis (AV01, AV08, AV10) and to define the calcite fabric of U-Pb dated layers (AV03, AV01; Fig. 6). Thin sections were analysed using a Zeiss Axio Scope A.1, at magnifications of 2.5x - 40x under plane and polarised light. Photomicrographs were taken with an attached Zeiss MrC5 digital camera and processed using Zeiss Efficient Navigation (ZEN) photo imaging software.

# 3.3. Uranium-lead

Samples were taken for U-Pb dating from two flowstones; the basal flowstone from Pit 5 and a capping flowstone of Pit 14 (Fig. 6). Once appropriate layers for U-Pb analysis were identified through phosphorimaging using a FUJIfilm BAS-1800 beta scanner (as per Pickering et al., 2010), small ( $\sim$ 5 mm³) blocks of flowstone were drilled out using a

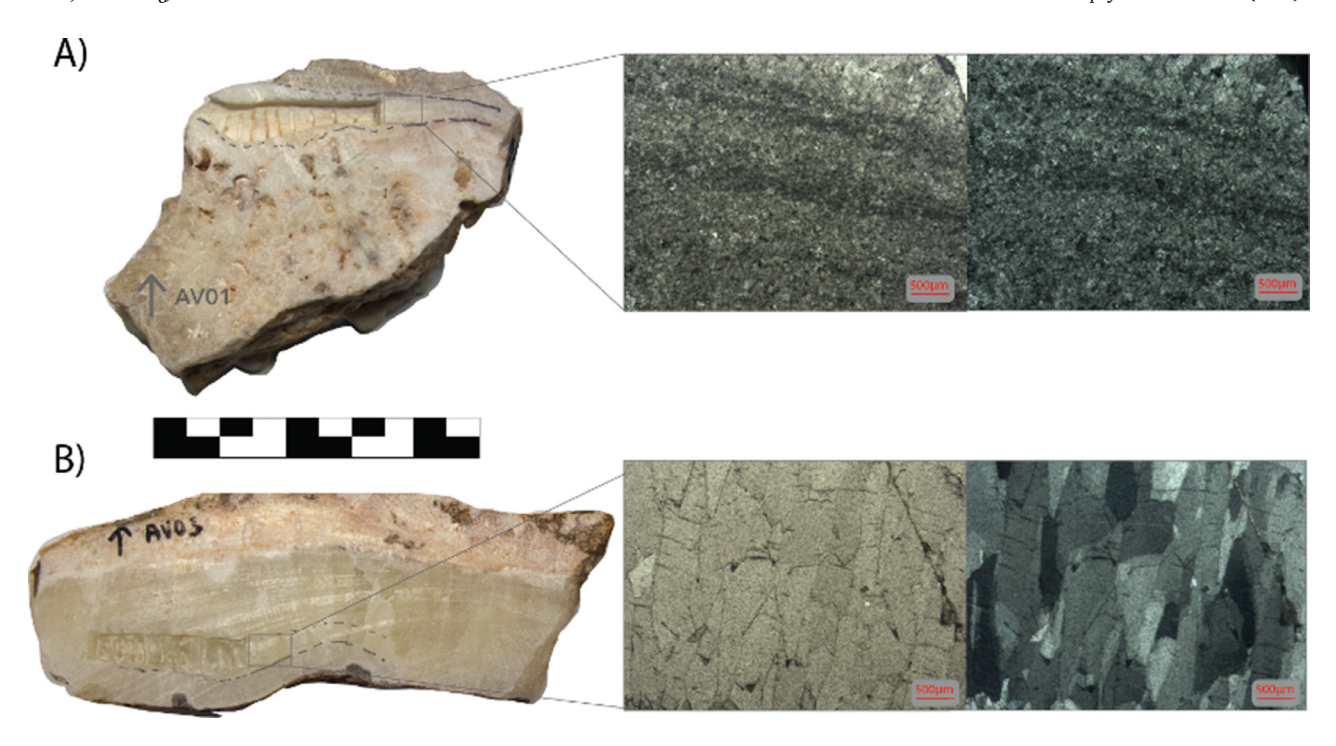


Fig. 6. U-Pb block samples and photomicrographs of fabric at dated layers. Scale bar represents 5 cm.

handheld hobby drill with a diamond tip burr. These blocks were etched in a weak HCl solution to remove any surface contamination and there after all handling took place in a class 360 clean laboratory. U and Pb isotopes were isolated and concentrated using standard ion chromatography and all measurements done on a Nu Instruments MC-ICP-MS, following protocols detailed by Woodhead et al. (2006) and Pickering et al. (2010; 2011b). Ages were generated using Tera-Wasserburg plots generated by Isoplot (Ludwig 2000) and finally calculated to include initial  $^{234}$ U/ $^{238}$ U disequilibrium (as detailed in Pickering et al., 2011b)

# 3.4. Rock magnetic and palaeomagnetic analyses

Palaeomagnetic analysis follows protocols outlined in Herries et al. (2020) and has been employed to identify the polarity of the geomagnetic field close to the time of sediment deposition, while corresponding rock magnetic tests determine the iron mineralogy and grain size of particles that carry the palaeomagnetic signal. The latter is critical to investigating the origin and stability of palaeomagnetic directions and to distinguish between components of primary (i.e. syn-depositional) and secondary (i.e. diagenetic) remanence. The sum of a sample's total magnetisation is the natural remanent magnetisation (NRM), and any secondary components or viscous remanent magnetisations (VRMs) are removed through demagnetisation to isolate the characteristic remanent magnetisation (ChRM) of palaeomagnetic subsamples.

Block samples from Pits 14, 5 and 8 were oriented *in-situ* using a Suunto compass and clinometer and removed following the hammer and chisel method. If needed, subsequent declination and dip corrections were made after drilling and analysis and the final declination for samples was corrected to true north (–17.776°) according to the 12th Generation International Geomagnetic Reference Field (British Geological Survey: http://www.geomag.bgs.ac.uk/gifs/igrf.html). Block samples were prepared for analysis at The Australian Archaeomagnetism Laboratory (TAAL) where 64 standard 20×25 mm cylindrical subsamples were drilled and cut using water-cooled equipment.

All palaeomagnetic measurements were made on an Advanced Geoscience Instruments Company (AGICO©) JR-6 Spinner Magnetometer (2.4 uAm sensitivity). To determine the ChRM, each subsample was

subjected to either a progressive thermal demagnetisation (TH<sub>D</sub>) in 20–40 °C steps to 700 °C using a Magnetic Measurements© (UK) MMTD80a shielded thermal demagnetiser (37 subsamples), or a 28–32 step alternating field demagnetisation (AF<sub>D</sub>) to 100 mT using an AGICO© LDA5 Alternating Field Demagnetizer (27 subsamples). TH<sub>D</sub> runs were undertaken in a zero-field cage. Unanchored ChRMs were calculated (Heslop and Roberts 2016) in Plotcore 2.1.0.0 using principal component analysis (Kirshvink 1980) with accepted best-fit components requiring a median angle of deviation (MAD) of <15° Mean directions for each sample block were determined using Fisher (1953) statistics in FISH2 with normal or reversed polarities defined on VGP-latitude directions under the following constraints: Normal: +90° to +45°; Intermediate: +45° to -45°; Reversed: -45° to 90°

Rock magnetic tests were undertaken on subsamples previously used for AFD or associated rock chips. These included room temperature mass-specific magnetic susceptibility ( $\chi$ ) measurements taken at low  $(\chi_{LF})$  and high  $(\chi_{HF})$  frequencies using a Bartington MS2 magnetic susceptibility metre at TAAL.  $\chi_{LF}$  was used as a proxy for magnetic grain concentration while the frequency dependency of  $\chi$  ( $\chi_{FD}$ %) was used to investigate magnetic grain size (domain state). Mineralogical characterisation was undertaken by estimating the curie temperature (Tc) of host magnetic minerals using two thermomagnetic methods. These included high temperature magnetic susceptibility ( $\chi$ /T) heating and cooling sweeps from room temperature to 700 °C while in air using a AGICO KLY-2 Kappabridge AC Susceptibility Bridge at the Institute for Rock Magnetism, University of Minnesota. A similar approach was utilised at the University of Liverpool Geomagnetism Laboratory (ULGL) where the sample's induced remanence (M) is monitored during heating and cooling from room temperature to 700 °C while in air (M/T) using a Magnetic Measurements Variable Field Translation Balance (MM-VFTB). As different parameters,  $\gamma$  and M cannot be analysed in the same way (Petrovský and Kapiĉka 2006), Tc estimates for M/T curves were derived from the Moskowitz (1981) approach using RockMagAnalyzer 1.1 (Leonhardt 2006), and those for  $\chi/T$  were calculated via the first derivative minimum of heating and cooling curves.

Isothermal remanent magnetisation (IRM) acquisition curves and backfields were acquired with a Magnetic Measurements© MMPM10 Pulse Magnetiser using a 38-step protocol to 1 T. Acquisition curves

**Table 1**Summary of facies identified for Bolt's Farm, including the ACC.

Facies	Description	Munsell rock colour (2009)	Interpretation
A	Large angular boulders, little matrix	5YR6/1(boulders) 10R 4/6 (matrix)	Gravity roof collapse
В	Massive sandy siltstone, few clasts, bone poor	10R 4/6 -10R 6/2	Catastrophic flood event (mid fan)
B1	Sandy siltstone, some clasts and bone	10R 4/6-10YR 7/4	Less intense rain event (mid fan)
С	Laminated, brown siltstone with fine sand. Bone rich	5YR 4/4-5YR 6/4	Winnowed equivalent of A (mid fan-distal)
D *	Brown to dark brown laminated, clay rich siltstone. Few clasts. Some bone, well preserved.	10R 3/ 4 - 5YR 2/2	Deposition of fines from gentle flowing water (distal)
Е	Flowstone	N9	Closed cave, wet external hydroclimate
F	Red brown to light brown, laminated siltstone and sandstone, some bone	10R 4/6 -10YR 7/4	Increasingly arid environment, aeolian and minor rain wash (mid fan)
G	Red brown silty sand, some bone	10R 4/6	Winnowed equivalent of F (distal)

 $D^*$  This model was developed for Bolt's Farm as a complex of <20 sites, Facies D is not observed within ACC.

**Table 2**Summary of petrographic analysis for samples from Pit 14 and Pit 5.

Sample	Locality	Lithology	Secondary	Depositional episodes	Facies	Depositional mode
AV01	Pit 5	Flowstone, clastic unit at top	No evidence	5	Е	Closed cave- allows unimpeded precipitation of flowstone.
AV08	Pit 14	Siltstone	No evidence	8	В	Catastrophic flood event associated, massive bedding. Less intense rain events deposit B1. Early stage cave open.
AV10	Pit 14	Laminated siltstone	Secondary calcite in voids	3	F	Fluctuating hydrological input, depositing alternating sandy and silty layers, general fining upwards trend. Late stage cave open, associated with increasing aridity.

were de-convoluted using MAX UnMix (Maxbauer et al., 2016) to characterise different coercivity components contributing to the IRM. Hysteresis loops were measured using a MM-VFTB at the University of Liverpool Geomagnetism Laboratory. Data was processed using RockMag-Analyzer 1.1 software (Leonhardt 2006). Low temperature magnetometry was also applied to pilot samples for mineral characterisation at the Institute for Rock Magnetism using Quantum Designs Magnetic Properties Measurement System (MPMS) XL and 5 s instruments. Samples were subjected to a 'sweep-cool-warm' measurement sequence, which involves imparting a room temperature (300 K) saturation isothermal remanent magnetisation (RTSIRM) to 2.5 T, and undertaking remanence measurements in 5 K intervals while cooling to 20 K. At 20 K another SIRM of 2.5 T is applied, and the remanence is measured on warming to 300 K.

# 4. Results

A combined U-Pb magnetostratigraphy for the three sites is presented in Fig. 4, with stratigraphic columns documenting the mode of deposition (externally derived clastic sediments vs flowstone). Facies for the site are presented in Table 1. Thin section analyses were carried out to assist in lithofacies identification (Table 2; Fig. 5) and to test the suitability of U-Pb samples (summarised in Table 3; Fig. 6) and palaeomagnetic samples (Table 4). U-Pb dates were produced for the basal and capping flowstone with Terra-Wasserberg plot shown in Fig. 7. Rock magnetic analysis shows that sample blocks preserve a stable magnetic record (Fig. 8) and palaeomagnetic results (Table 4; Fig. 9) show

a normal polarity through the sequence including direct analysis of fossil bearing layers. A reconstruction of cave infilling and related facies (Fig. 10) is presented in the context of previous models (Table 5).

# 4.1. Stratigraphy and petrographic analysis

The pits of the ACC preserve both clastic sediments (cumulatively referred to throughout the existing literature as 'cave breccia') and speleothem. The strata exposed across the three localities have been classified under a facies model adapted from Pickering et al. (2007) (Table 1), with five types of clastic sediment identified (Facies A-G). Facies A is classified by the presence of large clasts and boulders, Facies B by silty sandstone, Facies C by light brown bone rich siltstone with fine sand, Facies F is composed of laminated siltstone and sandstone and Facies G red brown silty sand. All speleothem material is classified as Facies E (Fig. 4).

Due to the extensive erosion and impact of mining, the sediment exposure at Pit 14 is discontinuous (Fig. 3A), but a composite stratigraphic section was compiled (Fig. 4). Facies E, defined by the presence of calcium carbonate precipitate, is present at the base of Pit 14 in the form of a sloping, laminated flowstone. This is followed by Facies A, characterised by large >30 cm - <1.5 m angular boulders of chert and dolomite. This unit is massive, clast supported with red brown medium grain sandy matrix. Few other clasts are present and little to no bone is preserved. This facies is only visible at the eastern edge of Pit 14 and transitions downslope into Pit 8. Succeeding this is Facies B composed of massive, brown to reddish brown matrix with few clasts and a yuggy texture.

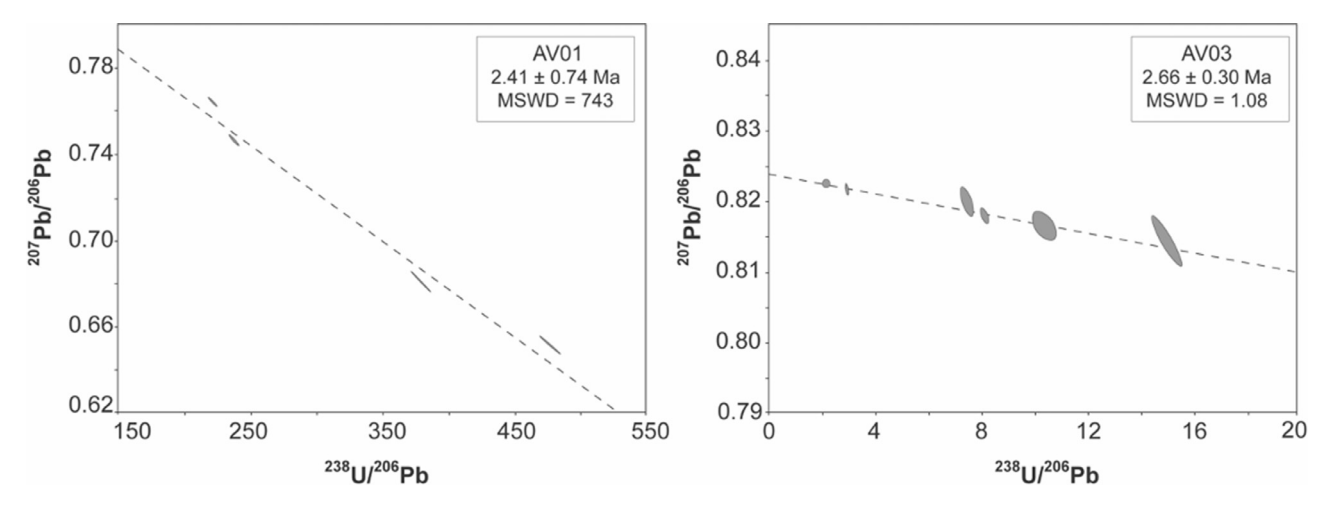
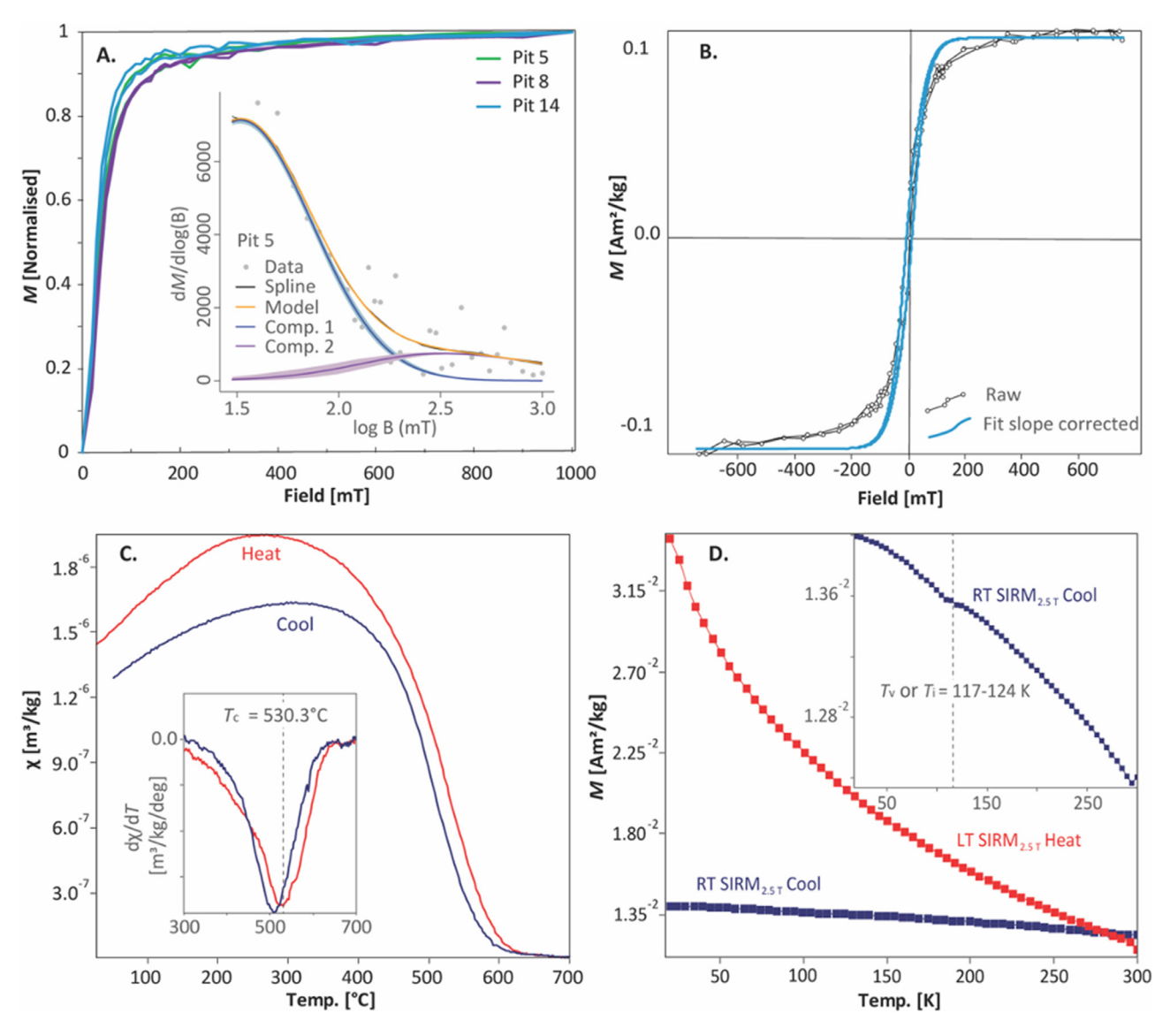


Fig. 7. Terra-Wasserberg plots for the basal (AV01) and capping (AV03) flowstones, ACC.



**Fig. 8.** Results of rock magnetic experiments. A) IRM curves for three pits, inset: unmixing reveals at least 2 magnetic components contributing to acquisition curve and B) Thermomagnetic curve for AV08 shows a Tc of 530.3 °C, indicating the presence of impure magnetite. C) Low temperature magnetometry shows subtle inversion close to Verwey transition. D) Pot -bellied hysteresis curve from AV09.

Table 3
U-Pb results for AV01 (basal) and AV03 (capping flowstone).

Sample	Conce U	ntratioon PB	<sup>238</sup> U/ <sup>206</sup> PB	%Er	<sup>207</sup> Pb/ <sup>206</sup> Pb	%Er	Cor.Coef.	<sup>238</sup> U/ <sup>204</sup> Pb	% Er	<sup>206</sup> / <sup>204</sup> Pb	%Er	Present <sup>234</sup> U/ <sup>238</sup> U	% Er	U-Pb (T-W Age)	±	%Er
AV01-1	1.08	0.0157	220.3	1.2	0.7639	0.2	-0.9999	4558.2	1.4	20.69	0.29	1.0036	0.4	2.410	0.739	30.7
AV01-2	0.98	0.0059	475.7	1.3	0.6516	0.5	-0.9987	11,578.4	1.8	24.34	0.57					
AV01-3	1.35	0.0106	373.5	0.6	0.6840	0.2	-0.9939	8635.2	0.9	23.12	0.35					
AV01-4	0.78	0.0104	236.2	1.2	0.7462	0.3	-0.9862	4977.7	1.5	21.08	0.31					
AV01-5	0.96	0.0074	380.7	1.2	0.6793	0.4	-0.9983	8869.3	1.6	23.30	0.51					
AV01-6	0.77	0.0052	458.8	4.2	0.7043	1.2	-0.9980	10,114.9	5.6	22.05	1.80					
AV01-7	1.15	0.0019	1162.2	2.5	0.3531	3.9	-0.9998	56,683.6	7.2	48.77	4.77					
AV01-8	0.82	0.0034	667.5	6.7	0.5466	4.5	-0.9996	20,337.5	12.4	30.47	6.02					
Ave.	0.99	0.0076														
AV03-1	0.02	0.0078	7.4	2.7	0.8199	0.2	-0.6864	143.6	2.9	19.41	0.38	1.0046	0.6	2.668	0.304	11.4
AV03-2	0.01	0.0177	2.9	1.3	0.8217	0.1	-0.5797	54.9	1.4	19.06	0.33					
AV03-3	0.02	0.0258	2.1	4.8	0.8225	0.0	-0.1062	40.5	4.8	19.11	0.37					
AV03-4	0.02	0.0075	8.1	1.6	0.8178	0.1	-0.6835	154.7	1.7	19.20	0.34					
AV03-5	0.03	0.0092	10.3	3.7	0.8165	0.2	-0.5256	198.8	3.8	19.29	0.45					
AV03-6	0.02	0.0042	14.9	3.2	0.8143	0.4	-0.9142	286.8	3.9	19.21	1.63					
AV03-7	0.02	0.0004	184.7	28.7	0.7121	7.9	-0.9997	3980.0	36.6	21.55	8.98					
AV03-8	0.01	0.0004	154.1	166.2	0.6494	66.5	-0.9998	3329.4	211.0	21.60	46.24					
Ave.	0.02	0.0091														

**Table 4**Results of palaeomagnetism for the ACC, presented stratigraphically.

Block	Location	Deposit	No	Dec	Incl	VGP	α95	k	$_{\chi} \mathrm{LF}$	$\chi { m FD}\%$	Polarity
AV01	Pit 5	Flowstone	3/5	323.6	-49.9	57.8	21.8	33	_	-	N
P802	Pit 8	Siltstone	4/4	4.7	22	52.7	36.5	5.3	2.6	10.3	N
AV02	Pit 5	Siltstone	7/8	337.6	-55.2	68.5	11.2	29.8	3.8	13.5	N
P501	Pit 5	Siltstone/Breccia	3/3	282.9	-48.4	22.9	30.3	17.6	6.5	11.3	I
P801	Pit 8	Breccia	5/5	323.5	-51.8	57.7	17.9	19.2	5.0	4.9	N
AV12	Pit 14	Siltstone	5/6	348.6	-43.5	79.7	17	19.9	7.3	14.3	N
AV08	Pit 14	Siltstone	5/7	351.8	-50	81.4	23	11.3	4.7	11.9	N
AV09	Pit 14	Siltstone	6/7	314	-46.3	49.1	21.8	10.4	5.6	12.5	N
AV05.1	Pit 5	Siltstone	5/7	332.4	-37.7	64.3	40.6	4.5	2.5	9.3	N
AV05.2	Pit 5	Siltstone	3/5	349.1	-49.1	79.6	33	14.9	3.5	10.2	N
AV10	Pit 14	Siltstone	3/7	332.6	-71.2	54.2	15.8	62	5.4	11.5	N

Clasts present are small <1 cm, the matrix consists of fine to medium sand and there is little to no preservation of bone. Where Facies B includes intercalated sandy units, which include some clasts <1 cm and preserve bone, it is referred to as Facies B1. At Pit 14 there is alternating units of bone poor Facies B and bone rich B1 arranged in a coarsening up sequence. These deposits are overlain by Facies F, which consists of interlaminated reddish-brown sandy silt and light brown sand. Clasts are present at base up to 1 cm, with a fining up sequence observed to top of unit. Laminations are generally planar, with bone bearing pebble lenses through the base and middle. Facies E is again observed at the top of the sequence in the form of a heavily eroded and or mined flowstone. Pit 14 represents a complete FBU with a package of clastic sediment sandwiched between two flowstones.

Pit 5 is located  $\sim$ 15 m north east of Pit 14 and is a small cavern with a preserved ceiling (Fig. 2; 3B). Along the back wall  $\sim$ 1.75 m of stratigraphy is preserved, with the overlying deposits recorded at an exposure at the entrance. Facies E is again noted at the base of this sequence as a flowstone overlying outcropping host rock dolomite. The flowstone is clear but poorly preserved towards the north. This is overlain with Facies C, a brown to light brown fossil rich siltstone, with generally bone poor fine to medium sandstone. Minor planar laminations are observed. This unit is succeeded by Facies B, which is interlaminated with Facies B1, preserving some microfossils. From the upper ceiling to the cave entrance Facies G is present. Facies G is matrix supported, generally massive and composed of reddish-brown sandy silt. A basal and upper sandy unit is associated with some planar bedding structures and preservation of fossil microfauna.

Pit 8 is located immediately east of Pit 14 and preserves approximately 3 m of strata, with  $\sim$ 1 m of host rock outcropping at the base and

extensive (>1 m) modern colluvium at the top of the sequence (Fig. 3C). As with the two other pits, Pit 8 contains Facies E at the base of the sequence, deposited on host rock. Facies A is present with the bulk of boulder material concentrated up slope towards Pit 14. Facies B is extensive at Pit 8, with some large clasts >15 cm clasts likely having been eroded from Facies A. Facies B at this location shows chaotic bedding and any clasts present have a random orientation. There is no evidence for intercalated Facies B1 at Pit 8. Facies G is again present at the top of the sequence, representing the finer portion of Facies F. Sediment is reddish brown sandy silt with minor bedding development suggesting deposition on a slope of ~20°. Facies E is present in the form of a small, thin flowstone the remainder of the sequence is modern colluvium.

Thin section analysis was carried out to further characterise the facies, and to assess the suitability of samples for U-Pb and palaeomagnetic analysis (Fig. 5; Fig. 6). AV01 is a flowstone sample which represents Facies E in Pit 5. The initiation of Facies B is observed in sample AV08 from Pit 14. AV10 from Pit 14 represents Facies F. Results for analysed thin sections are summarised in Table 2.

# 4.1.1. Facies E: flowstone

Fig. 5A, shows flowstone sample AV01, the basal flowstone. This sample has five units of growth with the lower four being composed of precipitated CaCO<sub>3</sub> (calcium carbonate) and the top a clastic unit cemented with calcite. The basal unit is low porosity composed of large equant calcite crystals with a thin detrital layer (Fig. 5A1). Unit 1 has an irregular basal contact, marked by a sharp change in crystal structure and is dominated by the presence of aragonite (Fig. 5A2) throughout and has an irregular contact with unit 2. Unit 2 is marked by a transition to microsparite with common voids and high porosity. Unit 3 is

Moriarty et al. (2000)			This Stud	y- ACC Resul	Pickering et al. (2019)			
Hydroclimate WET	Cave Closed	Sediment input  No clastic material. Flowstone growth is moderate and clean. Minor reworked clastic may be present	Facies E	Sample AV01 (basal) AV03 (Capping)	Cave Closed	Observed deposit Flowstone, mostly clear. Basal flowstone (AV01) has clastic material at top indicates cessation of flowstone growth. Capping flowstone is composed of mosaic to microcrystalline calcite and has a growth hiatus.	U-Pb ages @ base 2.410 ± 0.739 (3.180-1.670 Ma) @ top 2.668 ± 0.304 Ma (2.972-2.364)	Flowstone growth interval (FGI) @ base FGI1 (3.19-3.08 Ma) @ top FGI2 (2.83-2.62)
WET	Open	Clastic input low, bone high, if flowstone present it is contaminated with clastic and bone	В	AV08	Open	Red brown sandy siltstone, derived from catastrophic flood events. Generally massive, little bone.	-	SED1 (3.08-2.62)
WET	Open	Clastic input low, bone high, if flowstone present it is contaminated with clastic and bone	B1	AV09	Open	Red-brown siltstone, increasingly rich in bone following coarsening upward sequence. Derived from less intense rain events.		SED1 (3.08-2.62)
ARID	Open	High clastic input, low bone. No flowstones present, common laminated clastics.	F	AV10	Open	Brown to light brown laminated siltstone/ sandstone. Decreasing bone material follows fining up sequence to brown siltstone.	-	SED1 (3.08-2.62)
ARID	Closed	No clastic input, no flowstone growth. Erosive/ hiatus surfaces	-		-	-		=

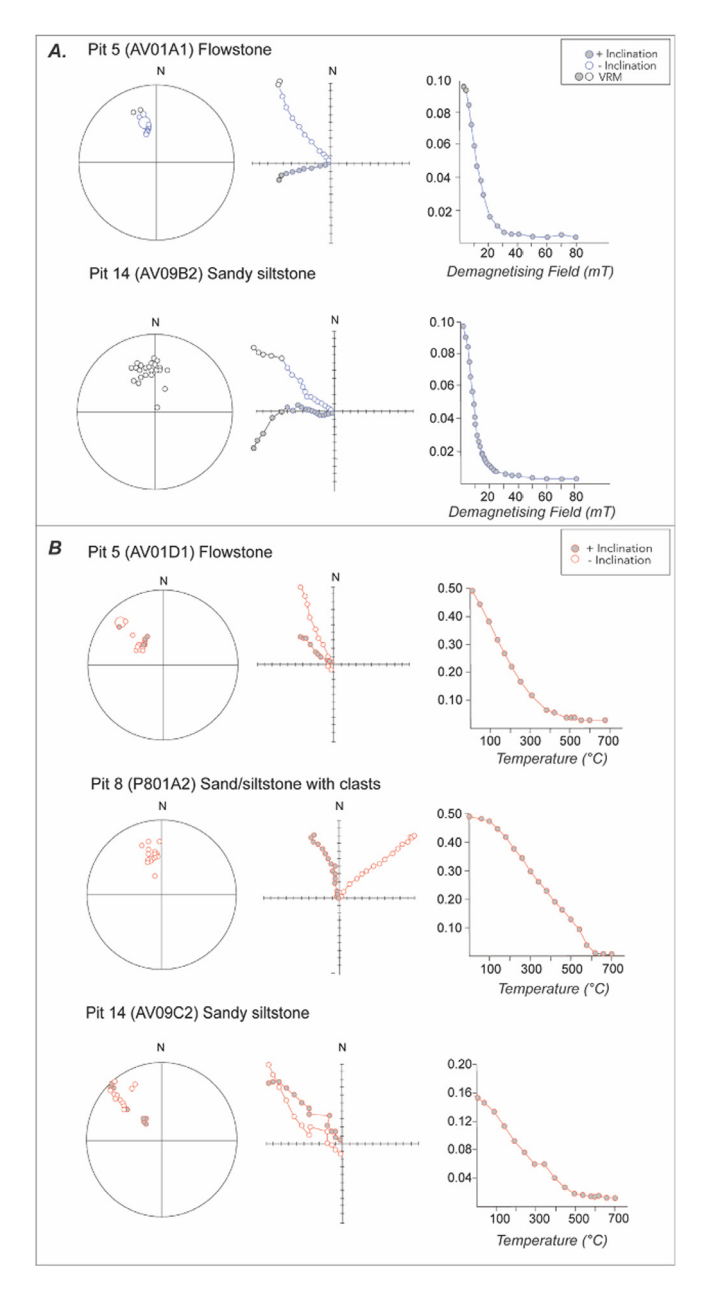


**Fig. 9.** Example of palaeomagnetic behaviours. Results show normal polarities for the three sites in both A) alternating field demagnetisation and B) thermal demagnetisation.

distinct, composed of microsparite with rare fine grained, poorly sorted sub angular to rounded quartz. This unit has a medium-high porosity with numerous voids, partially filled with secondary calcite. The top of unit 3 is marked by a dense micritic layer (Fig. 5 A3). The capping unit has an irregular basal contact and is marked by an increase in clay content, and a dominance of large (200–300  $\mu m$ ) angular to sub rounded quartz grains in a calcite spar cement (Fig. 5 A4)

# 4.1.2. Facies B: silty sandstone

AV08 is a vuggy siltstone, with seven low porosity units defined by differences in calcite abundance and crystal form and the presence and abundance of lithic grains (Fig. 5B). The basal unit is a matrix supported silt with poorly sorted angular to sub rounded quartz and chert grains. Up to 90% of lithic grains are quartz and chert <30  $\mu m$ , but large grains of chert up to 575  $\mu m$  are present at <1%. There is a sharp contact with unit 1, marked by a change in the silt matrix to a calcite cement (Fig. 5

B1). Unit 1 is matrix supported fine quartz and chert in equant calcite spar cement. This unit contains poorly sorted grains of quartz and chert, sub angular to sub rounded with common clay coatings noted. Unit 2 is matrix supported quartz and chert in a calcite and silt cement. Lithic grains of quartz and chert up to 115 µm in size with 50% <30 µm, rare bone is noted at less than 1% (Fig. 5 B2). Unit 3 is matrix supported fine lithic grains in an equant spar calcite cement. Poorly sorted, sub angular to sub rounded grains of chert and quartz ranging from  $20\,\mu m$ to 200  $\mu m$ , with grains <30  $\mu m$  present at 30%, >30–100  $\mu m$  present at 40% and grains >100 µm present at 10%, with the remaining 20% attributed to the matrix (Fig. 5 B3). Common clay coatings on grains are noted. Unit 3a is a subunit extending less than halfway through unit 3 and is composed of silt dominated by calcite infilled vughs and common angular to sub rounded quartz grains <100 µm present at 70% and grains 100-300 µm present at 5%. Unit 3 continues around and above the sub unit 3a, and there is a transitional contact from unit 3 to unit 4, a matrix supported quartz and chert in silt. Lithic grains of quartz and chert are poorly sorted, sub angular to rounded >100 µm in size with clay coatings. Common aggregates of clay are noted throughout. The capping unit consists of laminated silts and fine sands in a calcite microspar cement. Lithic grains consist of moderately sorted sub rounded quartz grains up to 100 µm with occasional bone fragments throughout (Fig. 5 B4).

### 4.1.3. Facies F: laminated siltstone and sandstone

AV10 is a laminated deposit which consists of three units of alternating silt and fine sands with varying amounts of calcite present as cement, representing winnowed sediments. The basal unit is matrix supported fine grained quartz in calcite microspar cement. Lithic grains of quartz 30- 10 µm are moderately sorted, sub angular to rounded with clay filling interstitial spaces. The top of the unit is discernible with a clear contact marked by clay deposit (Fig. 5 C1). Unit 1 is low porosity, matrix supported in calcite cement. The abundance of angular to sub rounded chert and quartz 100 μm-2300 μm, with only 20% 30-100 μm shows a change in mode of deposition, possibly a flood event. The top of the is unit marked with an irregular but clear sharp contact and decrease in clay content (Fig. 5 C2). Unit 2 consists of thick succession microlaminations of alternating units of fine sand with high clay content and fine sands with high calcite content. This unit is low porosity, moderately sorted with angular to rounded quartz, 50% lithic grains 100–250 μm, 20% 30-100 μm. Rare bone is noted throughout unit along with degraded drusy calcite spar infilling voids. A thick sandy unit can be seen in Fig. 5 C3 which shows a short-lived change in feeding sediment, contrasting with the microlaminations seen in Fig. 5 C4.

# 4.2. U-Pb ages

Petrographic analysis of the dated layers from AV01 and AV03 reveal primary growth fabrics. The U-Pb dated layer in AV01 is composed of fine, laminated calcite spar (Fig. 6), however, the upper undated portion shows abundant relict aragonite rays in secondarily precipitated calcite mosaic spar. The dated layer of AV03 is dominated by blocky columnar calcite (Fig. 6). While the undated portion of AV01 indicates evidence of diagenesis in its fabric, from the petrography of the dated layers of both AV01 and AV03 we predict that there has been no loss or gain of U-series isotopes through recrystallisation.

The concentration and isotope ratio data for AV01 and AV03 are summarised in Table 3 and Tera-Wasserburg plots are provided in Fig. 7. The initial U-Pb ages show an apparent age inversion with the basal flowstone (AV01) returning an age of  $2.410\pm0.739$  Ma, with the median age younger than that of the capping flowstone (AV03) at  $2.668\pm0.304$  Ma. However, both overlap within error and AV01 has a large error of 30% (typical U-Pb error range 5–10%), despite the fact that the uranium concentration is as expected at ~1 ppm (0.99 ug/g). However, uranium concentration was variable throughout the 8 aliquots (Table 3). While there is uncertainty on the  $^{234}$ U/ $^{238}$ U measurement, the

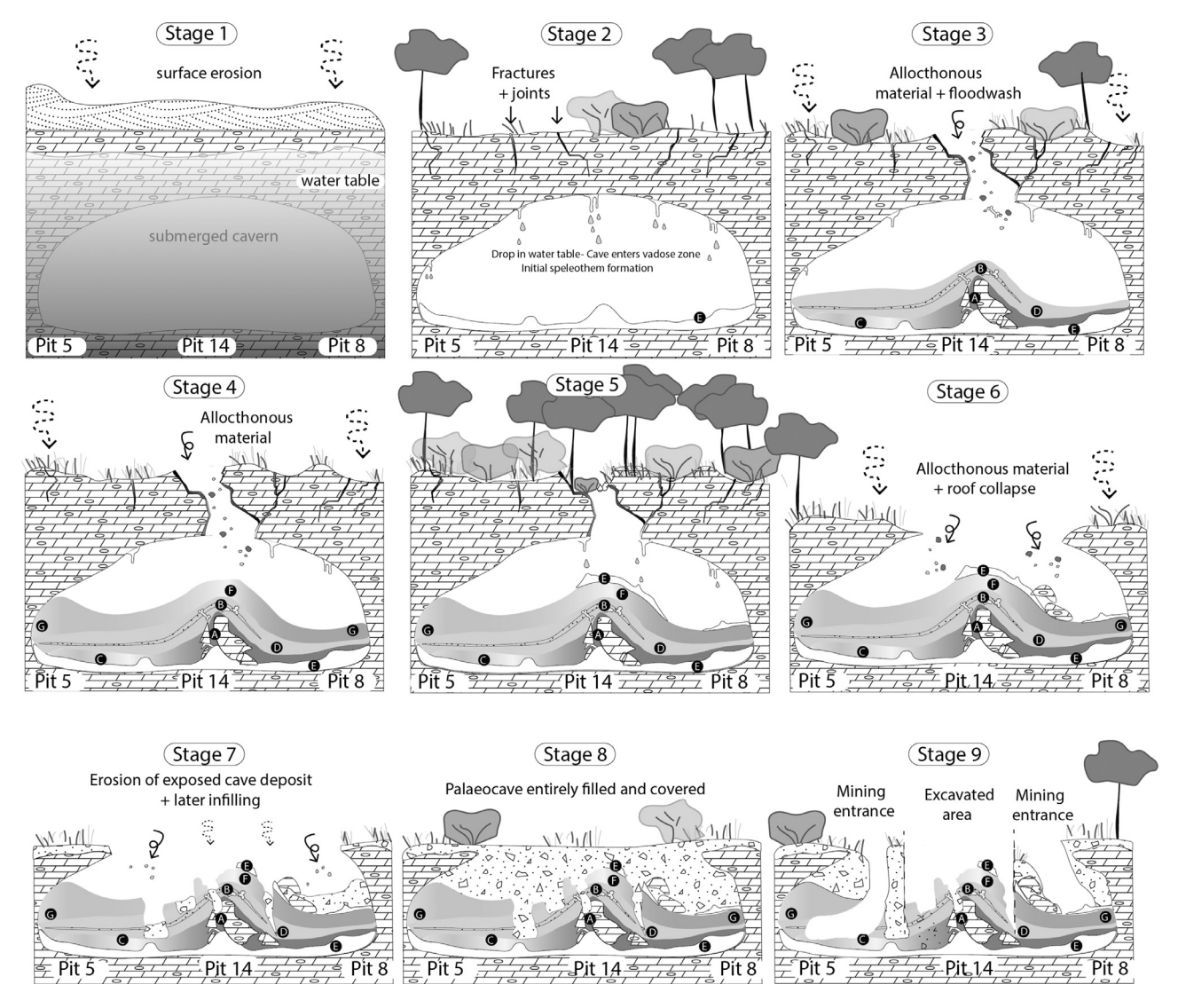


Fig. 10. Simple 9 Stage model of development for the Aves Cave Complex. The model moves from the dissolution of the cave (Stage 1) to initial speleothem formation (Stage 2) and the opening of the cave and deposition of allochthonous material (Stage 3, 4). A 'cave closed' scenario is shown in Stage 5, where increased vegetation obscures the cave entrance and increased effective precipitation reinitiates speleothem formation. Erosion and exposure of the cave deposits is seen in Stage 6 and 7, while infilling of the cave is seen in Stage 8. The modern representation of the apparent separate sites following mining activity and palaeontological excavation is shown in Stage 9.

large error on AV01 is most likely linked to scatter, with no ages intersecting the isochron (Fig. 7). No single points were eliminated, and it is possible that further aliquots could elucidate the scatter. The capping flowstone AV03 has an age of  $2.66\,8\pm0.304$  Ma, representing the minimum age for the deposit. This sample has an 11% error, linked to poorly constrained  $^{234}\text{U}/^{238}\text{U}$ , which can be attributed to very low uranium concentrations <0.05 ppm (0.02 ug/g). Ideally flowstones need around 1 ppm of U tom produce measurable amounts of U-series daughter decay products (Woodhead & Pickering, 2012).

# 4.3. Mineral magnetism

 $\chi_{\rm LF}$  values ranged from 2.5–6.3×10<sup>-6</sup> m<sup>3</sup>/kg suggesting a high concentration of ferrimagnetic grains present in palaeomagnetic subsamples across the three localities. Mean  $\chi_{\rm FD}$ % values were high at 10.93% within a range of 4.90–13.51% suggesting a significant proportion of these occur as ultrafine superparamagnetic to single domain (SP/SD) boundary grains (with the maximum value for natural samples at 16%; Dearing et al., 1996). IRM acquisition curves and hysteresis loops ex-

hibit minimal variation between the three Pits and are dominated by a low coercivity ferrimagnetism (Fig. 8). The bulk of the IRM is acquired at low fields prior to 100 mT (84–91%), and there is some resistance to 300 mT, suggesting the presence of at least two low coercivity components (Fig. 8A). Rapid acquisition of an IRM and pot-bellied hysteresis loops (Fig. 8B) (Tauxe et al., 1996) likely reflect the presence of SP/SD boundary grains in line with high  $\chi_{\rm FD}\%$  results, whereas the more stable component suggests the presence of stable single domain (SSD) ferrimagnetic grains (Walden et al. 1999). IRM curves also display a non-saturation component (Fig. 8A) indicative of high coercivity minerals, which likely relates to haematite, and potentially goethite, as shown in previous studies (Herries et al., 2018).

 $\chi$ /T and *M*/T curves (Fig. 8C) show that forms of magnetite dominate the subsamples, with Tc estimates ranging from 505 °C to 585 °C. Such phases are likely responsible for the low coercivity IRM and hysteresis properties observed. Additional evidence for magnetite is present via low temperature magnetometry, with subtle inflections close to the Verwey transition (Tv; ~120 K) shown in RT SIRM2.5 T cooling curves (Fig. 8D). A lowering of the Tc and remanence unblocking tempera-

tures observed during thermal demagnetisation (Fig. 9) are characteristic of Ti-substitution in magnetite, and thus we interpret the smoothing out of the Tv as relating primarily to Ti-effects and the presence of titanomagnetite, similar to a recent example from the Drimolen Makondo (Herries et al., 2018).

In summary, these results suggest that ACC samples across the three localities contain a mixture of SP/SD and SSD magnetite and impure Ti-magnetite, along with haematite and possibly goethite in some samples, but with the magnetic remanence being recorded within magnetite and titano-magnetite. SP/SD magnetic grains are likely to carry VRM overprints, whereas detrital SSD grains are capable for recording a post depositional remanent magnetisation (pDRM) parallel with the prevailing magnetic field. A low percentage of overall SSD grains, high SP/SD grains and a strong, but easily removed VRM, is a feature of many South Africa palaeocave sites (Herries et al., 2006; 2014; 2018 Dirks et al., 2010).

### 4.4. Palaeomagnetism

Palaeomagnetic results for Pits 14, 5 and 8 are presented in Table 4 with the bulk of Fisher (1953) mean directions assigned as normal polarity, with an isolated intermediate direction recorded midsequence in Pit 5. Demagnetisation behaviour was largely consistent across the three localities, with ChRMs isolated in the bulk of THD subsamples from 150 °C to their unblocking range at 580-600 °C (Fig. 9) which is suggestive of magnetite, and in some cases maghemite as the main remanence carrying minerals. Some subsamples exhibited much lower unblocking temperatures <400 °C (Fig. 9) indicative of Timagnetite or maghemite, although their final directions were consistent with those unblocking in the 580-600 °C range. This suggests that lockin time for different phases of detrital minerals was coeval. Consistent ChRM directions to TH<sub>D</sub> were obtained during AF<sub>D</sub> typically at 9-37 mT (Fig. 9). These further demonstrate the low coercivity nature of the subsamples, with average MDFs of 12 mT (and 260 °C for THD) and strong VRMs removed prior to the isolation of a ChRM (Fig. 9). Palaeomagnetic data from Pit 8 was more problematic compared to Pits 5 and 14, with only limited sampling undertaken due to a lack of suitable exposed stratigraphy (Fig. 4) and a notable dispersion amongst subsamples (Table 3). Fisher (1953) block means returned normal polarity results, with P801 ( $D = 323.5^{\circ}$ ;  $I = -51.8^{\circ}$ ) consistent with means of normal polarity blocks for Pit 5 ( $D = 335.7^{\circ}$ ;  $I = -48.0^{\circ}$ ) and Pit 14 ( $D = 336.8^{\circ}$ ;  $I = -52.8^{\circ}$ ). P802, while also exhibiting a normal polarity palaeolatitude, exhibits a high internal scatter (K = 5.3), lacks the dataset's consistent westerly declination and exhibits a positive inclination ( $D = 4.7^{\circ}$ ;  $I=22^{\circ}$ ), the latter of which is unusual for a normal dipole field from the site latitude. Such results may relate to palaeomagnetic recording biases within clastic karst deposits; for example, diagenetic dissolution and calcite recrystallisation have previously been linked to randomised directions occurring within portions of cave stratigraphy that are otherwise stable in magnetic polarity (Edwards et al., 2017; Herries et al., 2014). The dataset's only intermediate sample (P501) is also derived from the clastic component, and while true intermediate directions may be recorded during polarity transitions or excursions, the reliability of this data is questionable given the potential for depositional errors. Further, we note that the inclination record (-48.4°) of this sample is consistent with the site's normal polarity data. An isolated intermediate direction within a single-polarity dataset is unsuitable for magnetostratigraphic correlation, thus we consider the data here to reflect sediment deposition during a single normal polarity period.

# 5. Discussion

# 5.1. Three-dimensional sedimentary architecture and pit reconstruction

Most previous work on the cave deposits in the Cradle has focused on excavating and examining the fossil remains (Clarke 1998; Berger et al.,

2002; Partridge et al., 2003). While early work by Brain (1958) provided substantial insight into geological processes and potential links to changes in climate cycles, a lithostratigraphic approach has dominated the majority of Cradle sites (Wilkinson 1973; Partridge 1978; 1979; 2000; Clarke 1994; Partridge et al., 2003; Bruxelles et al., 2014; 2017). The work presented here is a deliberate departure from this approach and aims to highlight the importance of understanding the deposits through a sequence stratigraphic approach, combined with facies description.

Due to the inland location of the ACC on a stable craton, changes in sea level and tectonic activity would have played little to no role in changing sediment input over the last 3 Ma (Pickering et al., 2019). Consequently, drivers of changing sedimentation in the region must be linked to climate (Brain 1995; Ayliffe et al. 1998; Moriarty et al. 2000; Pickering et al., 2007; 2019). The presence of flowstones within cave environments has been linked to increased effective precipitation, along with generally closed cave conditions, and the intercalated sediment deposits must relate to drier periods (Ayliffe et al. 1998, Moriarty et al. 2000, Pickering et al., 2007; 2019). Very simply, the deposits under consideration here consist of a basal flowstone, a package of clastic sediments and a capping flowstone, suggesting a wet-dry-wet climate cycle is represented. While the basal flowstone is noted in all three Pits, the capping flowstone is sparse, occurring only in the south east of Pit 14 and south west of Pit 8. The capping flowstone is absent from Pit 5 and we suggest three possible contributors: Firstly, it is suggested here that the basal flowstone formed while the cave was still closed (FGI1), however the cave had developed an entrance by the time the capping flowstone was formed (during FGI2). The opening of the cave, while possibly obscured during FGI2 may have inhibited extensive flowstone growth as was seen in FGI1 with the basal flowstone. The second possibility is that FGI2 at ACC may have been less wet than FGI1, meaning that the flowstone did not fill the entire cave floor due to there being less flowing water. However, it should be noted that regionally the current data suggests more speleothems are forming during FGI2 than FGI1 (Pickering et al., 2019). Additionally, as with most other caves in this area, the deposits at Bolt's Farm were heavily affected by 19–20th Century lime mining, subsequently the third hypothesis is that there was a capping flowstone present at Pit 5 which was mined away.

By applying similar facies models to those used by Kos (2001) and Pickering et al. (2007) and producing composite stratigraphic sections for each locality (Fig. 4), it is possible to determine links between the three deposits, and how they fit with prior models (Table 5). A cartoon reconstruction (Fig. 10) shows a simple model of formation for the ACC, showing 9 stages of development through time. During stage 1 a cavern is dissolved by a high water table, as surface erosion strips the overlying karoo sediments and exposes the karst landscape. Following a drop in the water table, the submerged cavern is drained, and the cave enters the vadose zone. During this period, Stage 2, initial speleothem formation occurs with a large flowstone filling the cave floor (FGI1). A sinkhole opens an aven or vertical entrance to the cave, depositing Facies A (ceiling collapse). During Stage 3, allochthonous material can enter the cave for the first time and we see development of Facies C, the distal equivalent of fine sediments associated with Facies A. The deposits of Facies B formed during Stage 3 represent alternating catastrophic flood events (massive, bone poor) and less intense rain events (minor lamination, bone present) as B1. Such events would have deposited large amounts of sediment into the system which accounts for their extensive lateral range. The presence of macrofossils within this facies follows the hypothesis of Moriarty et al. (2000). This same model would suggest that increasingly arid conditions are associated with the deposits of Facies F (Stage 4). Additionally, lamination of clastic sediments associated with arid conditions and increased mobility of sand (Moriarty et al. 2000) are commonly observed within this facies (Fig. 4; Fig. 5C). Facies G present in both Pit 5 and 8 represents the distal equivalent of Facies F. Stage 5 is marked by a shift in hydroclimate, with increased effective precipitation and vegetation density around the entrance to the cave.

This vegetation and possibly some rockfall partly obscure the entrance to the cave, meaning that allochthonous material cannot easily enter and flowstone formation switches on again (FGI2). Following a return to more arid conditions, a period of erosion further lowers the ground surface and opens up the cave entrance in Stage 6 exposing the cave deposits. The deposits themselves are slowly eroded and eventually filled with colluvium in Stage 7 until the entire opening is filled and no longer exposed in Stage 8. The modern expression of the site is shown in Stage 9, where the action of mining has exposed much of Pits 5 and 8 and further palaeontological excavation has revealed much of the remaining deposits of Pit 14.

# 6. Biochronology

A number of species have been recovered from ACC (Pit 14) during recent excavations including specimens of *Crocuta* cf. *ultra*, cf *Parahyaena*, cf *Chasmaporthetes*, *Dinofelis*, *Panthera* cf. *leo*, *Panthera* cf. *pardus*, cf *Caracal*, *Felis Sylvestris*, *Canis* cf. *mesomelas*. *Raphicerus*, *Oreotragus*, *Connochaetes gentryi* and *Antidorcas recki* (Gommery et al., 2016). Many of the carnivores are not biochronologically sensitive and occur from the Pliocene to the present day. *Crocuta ultra*, *Canis mesomelas*, *Panthera leo*, *Panthera pardus* all occur in South Africa from Sterkfontein Member 4 (Werdelin and Peigné 2010), although *P. pardus* is also found in the Hrdlicka HE deposits (YRSS) at Taung tentatively dated to sometime between 2.58 and 1.95 Ma (McKee 1993; Herries et al., 2013) and in Sterkfontein Member 2, which could date to as early as 3.7 Ma (Werdelin and Peigné 2010; Granger et al., 2015), but could be younger than 2.8 Ma (Kramers and Dirks 2017). These species are known from earlier Pliocene deposits in eastern Africa (Werdelin and Peigné 2010).

Antidorcas recki is known from the 3.44 Ma old Shungura Formation Member B and younger deposits across eastern Africa, ultimately becoming common in terminal Pliocene deposits such as the 2.66 Ma old Upper Ndolyana Beds at Laetoli (Gentry 2010). In South Africa the species is first known from Sterkfontein Member 4 between 2.61 and 2.07 Ma ago and Drimolen Main Quarry between 2.04 and 1.95 Ma (Herries et al., 2020; Pickering and Herries 2020). Gommery et al. (2016) do not provide detailed measurements or descriptions to support the occurrence of A. recki, but if confirmed then it's occurrence at ACC would slightly extend the first appearance date of the species in South Africa (Supplementary Figure 1).

Connochaetes gentryi is known from the Upper Burgi Member of the Koobi Fora Formation to the Natoo Member of the Nachukui Formation in Kenya where it occurs between ~ 2.5 and 1.6 Ma (Harris 1991; Vrba 1995), Konso Intervals 1 and 3 between 1.9 and 1.6 Ma (Suwa et al., 2003), and Melka-Kunturé between 1.7 and 1.4 Ma in Ethiopia (Fiore and Tagliacozze 2004; Geraads et al., 2004) and Olduvai Gorge Beds 1 and 2 between 2.0 and 1.7 Ma (Deino 2012). In South Africa it has been tentatively identified from Member 2 of Kromdraai (1.95-1.78 Ma; Fourvel et al., 2016; 2018, Thackeray et al., 2002). This species has generally been used to suggest much younger ages for deposits when used for biochronology, although it has also been tentatively identified from northern localities in the Chiwondo Beds of Malawi between ~3.5 and ~2.0 Ma, again based on biochronology (Bromage et al., 1995). Gommery et al. (2016) do not provide detailed measurements or descriptions to support the occurrence of Connochaetes gentryi at ACC, just noting that "the dental remains coincide with that of C. gentryi. If this species is confirmed then the specimens from ACC would represent some of, if not the earliest yet recovered (Supplementry Fig. 1).

Pickford and Gommery (2016) describe new fossil material from ACC (Pit 14) attributed to the suid species *Notochoerus capensis* (Broom 1925) noting that this species is also found at the Makapansgat Limeworks (3.03–2.61 Ma; Herries et al., 2013). Ewer (1958) first described *Notochoerus* specimens from the Makapansgat Limeworks and referred them to *Notochoerus euilus*, a species known from the Turkana Basin between 6.5 and 1.9 Ma. Ewer (1958) specifically noted how different the material was from *N. capensis* and suggested the resurrection of the genus

Gerontochoerus (Leakey 1943) as a subgenus of N. euilus. In comparison, Cooke (2005) attributed these specimens to the later species Notochoerus scotti, also found in the Turkana basin between 4 Ma down to about 1.5 Ma (Rannikko et al., 2017). Pickford and Gommery (2020) instead suggest that the eastern African forms should be in the genus Gerontochoerus and that the ACC material should be referred to as Notochoerus capensis. Pickford et al. (2019) suggest that the Makapansgat specimens should instead be referred to Gerontochoerus scotti, removing any association between ACC and the Makapansgat Limeworks in terms of this species. The type specimen of Notochoerus capensis (Broom 1925) comes from undated deposits in South Africa (Longlands). Notochoerus capensis has been identified at Lee Adoyta in the Ledi-Geraru area, Ethiopia between ~2.8 and <2.5 Ma (Lazagabaster et al., 2018a) and Pickford et al. (2019) note that these are similar to those from ACC and the type specimen of this species, but not those from eastern Africa.

Cooke (1993) identified additional suid material from ACC (Pit 14), referring it to Potamochoeroides shawi. Cooke (1993) attributed a juvenile fossil from Sterkfontein Type Site (Member 4) to this species, noting its clear association to specimens from the Makapansgat Limeworks (Ewer 1958). Cooke (2005) later suggested that the genus Potamochoeroides should be abandoned and the species Metridiochoerus shawi instead used as a species name for the early stage in the evolution of Metridiochoerus as found at the Makapansgat Limeworks. Pickford and Gommery (2016), (2020) describe new fossils of suid species from ACC and instead referred these and previous fossils described by Cooke (1993) to Potamochoeroides hypsodont, the species first described from the Makapansgat Limeworks by Dale (1948), thus continuing to retain the genus Potamochoeroides. Others (Harris and White 1979; Rovinsky et al., 2015) have favored the simpler use of defined stages (I, II, III) within the evolution of the suid species Metridiochoerus andrewsi, a species still retained by Pickford as found at younger post 2 Ma sites (Adams et al., 2007; Pickford 2013). White et al. (2006) have suggested the formal recognition of three chronospecies, comprising M. shawi (stage I), M. jacksoni (stage II), and M. andrewsi (stage III). Despite differing views as to what genus and species the fossil material from Bolt's Farm and the Makapansgat Limeworks should belong it is clear that all authors agree that the material from the Makapansgat Limeworks and ACC are the same taxon.

Stage I M. andrewsi (M. shawi/P. hypsodont) is found at the Makapansgat Limeworks Member 3 (3.03-2.61 Ma; Herries et al., 2013), Drimolen Makondo (~2.61 Ma; Rovinsky et al., 2015, Herries et al., 2018), Sterkfontein Member 4 (2.61-2.07 Ma; Pickering and Herries 2020) and ACC in South Africa, and as early as the Unso Formation in Ethiopia at 3.4 Ma (White et al., 2006). In South Africa, Stage III M. andrewsi is found at younger post 2 Ma sites like Malapa (M. cf. andrewsi; ~1.98 Ma), Gondolin (~1.8 Ma), Swartkrans (1.9-1.0 Ma) and Kromdraai A (Adams et al., 2007; Herries et al., 2009; Lazagabaster et al., 2018b, Pickering et al., 2019). Very little is known of the intervening period covered by Stage II M. andrewsi (M. jacksoni) in South Africa because few sites can be confidently dated to the period between 2.6 and 2.0 Ma or have not yielded fossils attributable beyond Metridiochoerus sp. (Reynolds and Kibii 2011; Herries et al., 2020). The only exception is the single juvenile specimen Cooke (1993; STS 3074) attributed to Stage I M. andrewsi (M. shawi) at Sterkfontein Member 4 (Type Site). This specimen represents the last appearance date of Stage 1 in South Africa. However, given the fact that fossils from Member 4 accumulated over a long period of time between 2.61 Ma and 2.07 Ma the last appearance date is not well defined. This specimen may have come from deposits dating to the earlier part of this period but given that Stage III M. andrewsi is not seen in South Africa until sometime between 1.98 to 1.8 Ma the last appearance date is hard to define. The first appearance of the species is complicated by the fact that few Pliocene sites exist in South Africa and there are no confirmed deposits that are as early as the Unso Formation where this species first occurs in eastern Africa (Pickering et al., 2019). The age of the Makapansgat Limeworks deposits also remain tentative due to the fact only palaeomagnetism and biochronology have been applied to the

site. However, it is not younger than 2.61 Ma. In eastern Africa Cooke noted that a specimen from the upper layers of Shungura Formation unit B (above B-10) represented *M. shawi* and was comparable to the Makapansgat Limeworks specimens. This layer dates to between 3.03 and 2.61 Ma. By late unit C times, ~2.58 Ma *M. jacksoni* is present. *M. andrewsi* first occurs in upper Unit G that occurs around 2.20 to 1.95 Ma (Kidane et al., 2014).

Overall, this highlights the problems of using biochronology in South Africa where so few confirmed Pliocene fossil deposits occur between Langebaanweg at 5.2 Ma (Roberts et al., 2011), located in the very south-west of South Africa and the Makapansgat Limeworks at 3.03-2.61 Ma in the very north of South Africa (Herries et al., 2013). Additionally, confusion remains over the taxonomy of critical species as many papers provide species lists for sites rather than full descriptions and comparative data. The species identified from ACC highlight the importance of research on this time period, as well as the need for radiometric dating and chronological models not based on biochronology. Further refinement of chronological models for the age of the Makapansgat Limeworks, ACC (and other sites at Bolt's Farm) and Sterkfontein, as well as the discovery of new sites in the late Pliocene and earliest Pleistocene like Drimolen Makondo are critical for understating the relationship of these sites, the evolution of the various taxa represented at the sites, as well as their first and last appearance dates in the region.

### 6.1. Combined age determination

A final age determination is reached through the combination of all multi-disciplinary data (U-Pb, palaeomagnetism, biochronology) available to construct a magnetostratigraphy for ACC (Fig. 4). Given the overall consistency in polarity, palaeomagnetic data supports Pits 14, 5 and 8 forming as part of a single cave undergoing sedimentary infill during a period of normal polarity. While the median age of the basal flowstone (2.410  $\pm$  0.739 Ma) would place it within the reversed polarity Matuyama Chron, error on the U-Pb age (30%) covers a range of normal and reversed polarity magnetozones (Fig. 4). Taking into account the corresponding normal polarity of this flowstone, complete paucity of reversals throughout the sequence, and the capping U-Pb age at  $2.668 \pm 0.304$  Ma, these suggest deposition occurred during C2A1.1n (3.03–2.61 Ma) of the Gauss Chron. If the large error range on the basal flowstone is taken into account, it is an outside possibility that the deposits date to the slightly earlier C2An.2n (3.21-3.12 Ma) within the normal polarity period between the Mammoth and Kaena SubChrons, but this is unlikely. Moreover, the occurrence of species with first appearance dates younger than this make its assignment to the period between 3.03 and 2.61 Ma even more likely and suggest an age close to that of the capping flowstone at  $\sim$ 2.67 Ma.

# 6.2. Regional implications

The normal polarity of the sediments and the capping flowstone age date the fossil deposits of the ACC to older than  $2.668 \pm 0.304$ Ma, with the basal flowstone most likely forming at the end of Pickering et al. (2019)'s FGI1 (3.19-3.08). This would make the basal flowstone at ACC (Pit 5) slightly younger than HL1 (basal fs) at Hoogland (3.15  $\pm$  0.24 Ma). The capping flowstone from ACC (Pit 14) is dated to  $\sim$ 2.67 Ma forming towards the end of FGI2 ( $\sim$ 2.8–2.6 Ma). As argued above, the speleothems represent wetter external conditions; this is supported by a number of other flowstones which formed contemporaneously within the region during FGI2. These are, the basal speleothems at the Drimolen Main Quarry and Drimolen Makondo at ~2.67 Ma (Herries et al., 2018; Pickering et al., 2019; Herries et al., 2020), and the speleothem underlying Sterkfontein Member 4 (Pickering et al., 2019). This is not surprising, as in an area as small as the Cradle ( $\sim 10 \times 15 \text{ km}^2$ ) we would expect caves to experience the same hydroclimate and thus record deposits of the same age. This wet phase at ~2.6 Ma is also recorded by the capping flowstone of the Makapansgat Limeworks Member 3 deposits at ~2.61 Ma (Herries et al., 2013) and tufa also appears to have grown during this period at Taung (Herries et al., 2013). This is a period that is likely represented at Makapansgat Limeworks (parts of Member 2 west) and Taung pink claystone-siltstone (PCS) (Hopley et al., 2013), although this material could be much closer to 2.61 Ma. Deposits of this age are also represented by deposits below what is classically defined as Member 4 at Sterkfontein and has been defined as Member 3 by Partridge (2000) and Member 2 (excluding Silberberg Grotto) by Pickering and Kramers (2010). Very little is known about this deposit and its fossils. The fossil deposits at Hoogland may cover this time period, although like Makapansgat Limeworks and Taung no radiometric ages exist for the site (Adams et al. 2010).

While much has been made of their complexity (Bruxelles et al., 2014; 2017; Braga et al., 2017), it is argued here that externally derived sedimentary cave deposits follow the usual, hydrodynamic sorting of their fluvial counterparts (Miall 2014). As such, more coarse deposits occur proximally at and around the cave entrances, be these vertical or lateral; these deposits are then winnowed and have finer grained, distal equivalents which form contemporaneously in the deeper reaches of the cave (Brain 1967; Bosák et al., 2003; Lacruz et al., 2002; Pickering et al., 2007; White 2007). Due to limited exposures of these deposits, a solely lithologic classification system may identify these as two separate 'Members', emplacing a temporal bias, which does not accurately reflect the nature of deposition. An example of the potential errors associated with a lithostratigraphic system can be seen from the Makapansgat Limeworks, where Latham et al. (1999; 2002; 2003) showed that parts of a coarse clastic deposit (termed Member 4) were contemporaneous with a finer grained distal sediment (Member 2) and a fossil bearing breccia (Member 3). This affected the magnetostratigraphic age estimates for the site (McFadden et al., 1979) which had previously considered these three deposits as temporally restricted, when they are chronostratigraphically coeval.

Building on the work of Latham et al. (1999; 2002; 2003) Herries et al. (2006) used a sediment/flowstone approach at Buffalo Cave, in the Makapansgat Valley, defining 'phases' of speleothem sandwiching clastic sediment formation. Pickering et al. (2007) working at Gladysvale Cave, argued that this chronostratigrahic FBU approach circumvents the lithology-based issues of sediment association and dating. With initially U-Th and later U-Pb dating of basal and capping flowstones, Pickering et al. (2007; 2011a; 2011b; 2019) could then provide maximum and minimum ages for FBUs and constrain the periods of time represented by the flowstones themselves. Lacruz et al. (2002) were the first to apply a sequence stratigraphic approach to the external deposits preserved at Gladysvale Cave. The work of Pickering et al. (2007) continued this practice, after Kos (2001) of sediment classification in South African caves and produced a clear facies model.

While the application of sequence stratigraphy and the use of FBUs has been debated (Bruxelles et al., 2014; Stratford et al., 2014; Granger et al., 2015), arguments have largely been centred around the existence of intrusive flowstones. However, at Bolt's Farm, we see no evidence for the flowstones being intrusive; on the contrary, we observe a conformable sequence of flowstone and sediments. Furthermore, the petrographically the flowstones show no sign of diagenesis, meaning that not only are they in sequence, they have not undergone any post depositional alteration and therefore preserve a depositional age.

The model outlined in Pickering et al. (2007) is further supported the results presented here from the ACC. We argue that this model, of sediments sandwiched between flowstones to form a FBU, within which the lateral variation of depositional facies can be identified and related to changes within the cave and external sediment supply, is applicable to most vertical entrance palaeokarst sites in the Cradle. While site-specific nuances will also be present, these can be accommodated within this general model. The advantages of this approach are well demonstrated by this work at Bolt's Farm: we were able to describe and link together three separate deposits and reconstruct their formation as a single entity.

Within this stratigraphic and sedimentary framework, we were then able to date the flowstones underlying and capping the sequence, as well as use the palaeomagnetic signal to constrain the age to between 3.03 and 2.61 Ma.

# 7. Conclusions

At 3.03-2.61 Ma, the ACC represents one of the oldest directly dated fossil-bearing palaeokarst deposits in the Gauteng exposures of the Malmani Subgroup. The facies model applied here indicates that these sediments were deposited under a single entrance, located above Pit 14. Pit 8 represents part of the talus slope deposit and Pit 5 contains distal sediments. The apparent age inversion and large error range shown on the basal flowstone illustrates the limitations of U-Pb dating and the necessity of taking a multi-disciplinary approach to the dating and reconstruction of Plio-Pliocene aged sites. This is especially important where the sites preserve biochronologically indicative species, so that the age estimates for these may be better refined for the South African context. The use of palaeomagnetism provides continuity to the sequence and helps to refine the age of the basal flowstone creating a chronology for the deposits of the Aves Cave Complex. This research has shown how facies interpretation can be used to improve our understanding of palaeokarst systems, showing for the first time that currently discrete Cradle deposits were originally connected as part of a single cave system. This broader depositional understanding is of the utmost importance for providing context to recovered palaeontological material. Future research should focus on the unexcavated material between Pit 14 and Pit 5 to test the hypothesis presented here.

# **Declaration of Competing Interest**

The authors declare that there are no significant competing financial, professional or personal competing interests that might have influences the presentation of the work presented in this manuscript.

# Acknowledgements

Field work detailed here was undertaken as part of South African Heritage Resource Agency (SAHRA) Permit ID866, Ref No. 9/2/233/0032 and funded by an Australian Research Council Future Fellowship (FT120100399) and Discovery Grant (DP170100056) to AIRH, as well as La Trobe Humanities and Social Sciences Internal Research Grant Scheme #2017-1-HDR-0009 to TRE, #2017-1-HDR-0017 to TLM and NRF AOP grant 150924142990 to RP. We thank current and past permit holders (2016-2019); Stephanie Potze and Dominique Gommery (PermitID 892, 866), James Brink, Lazarus Kgasi and Domique Gommery (Permit ID 2672,2673). Special thanks to Lazarus Kgasi for access, Paul Penzo-Kajewski and Brian Armstrong for assistance in the field. The landowners, J. Klinkert, J. Gaylord, M. Gaylord permitted to access sites. The bulk of rock magnetic measurements were undertaken at TAAL, with additional measurements made at the Institute for Rock Magnetism (IFRM), University of Minnesota, and at the University of Liverpool Geomagnetism Laboratory. Components of the rock magnetic experiments were conducted during a Visiting Research Fellowship to T. Mallett at the IFRM, supported through the National Science Foundation, USA. We thank Dario Bilardello, Mike Jackson and Joshua Feinberg for their assistance and advice while measuring at the I<sub>F</sub>RM. We thank Norbert Plate of iQlaser (http://www.iqlaser.co.za) for the provision of aerial imagery. Thin sections were prepared by Adelaide Petrographics, Australia and David Wilson at University of Cape Town. We thank Alex Blackwood for assistance in figure preparation. This work was conducted as part of PhD research by TRE at La Trobe University and was supported by the Research Training Fund Scheme. Funding was also received from the Australian Research Council DE120102574 to R. Pickering.

### Manufacturer details

Bartington instruments, Oxen, United Kingdom.

AGICO, Brno, Czech Republic.

Magnetic Measurements, Aughton, United Kingdom.

Quantum Designs, San Diego, CA, United States of America.

# Supplementary materials

Supplementary material associated with this article can be found, in the online version, at doi:10.1016/j.ringps.2020.100005.

### References

- Adams, J.W., Herries, A.I.R., Conroy, G.C., Kuykendall, K., 2007. 'Taphonomy of a South African cave: geological and hydrological influences on the GD 1 fossil assemblage at Gondolin, a Plio-Pleistocene paleocave system in the Northwest Province, South Africa. Quat. Sci. Rev. 26, 2526e2543.
- Adams, J.W., Herries, A.I.R., 2010. Initial fossil discoveries from Hoogland, a new Pliocene primate-bearing karstic system in Gauteng Province, South Africa'. J. Hum. Evol. 59 (6), 685–691. doi:10.1016/j.jhevol.2010.07.021.
- Ayliffe, L.K., Moriarty, K.C., Wells, R.T., Marianelli, P.C., Hellstrom, J.C., McCulloch, M.T., Mortimer, G.E., 1998. 500 ka precipitation record from southeastern Australia: evidence for interglacial relative aridity. Geology 26 (2), 147–150. doi:10.1130/0091-7613.
- Berger, L.R., Lacruz, R., De Ruiter, D.J., 2002. Revised age estimates of Australopithecusbearing deposits at Sterkfontein, South Africa. Am. J. Phys. Anthropol. 119 (2), 192– 197. doi:10.1002/ajpa.10156.
- Berger, L.R. De Ruiter, D.J., Churchill, S.E., Schmid, P., Carlson, K.J., Dirks, P.H G M., Kibii, J.M. (2010) 'Australopithecus sediba: a new species of Homo-Like Australopith from South Africa', 328(April). doi: 10.1126/science.1184944
- Berger, L.R, et al., 2015. *Homo naledi*, a new species of the genus *Homo* from the Dinaledi Chamber, South Africa. Elife 4, 1–35. doi:10.7554/elife.09560.
- Bosák, P., Pruner, P., Kadlec, J., 2003. 'Magnetostratigraphy of cave sediments: application and limits'. Stud. Geophys. Geodaet. 47, 301–330.
- Braga, J., Thackeray, J.F., Bruxelles, L., Dumoncel, J., Fourvel, J.B., 2017. 'Stretching the time span of hominin evolution at Kromdraai (Gauteng, South Africa): recent Discoveries'. Comptes Rendus Palevol. 16, 58–70.
- Brain, C.K., 1958. The Transvaal Ape-Man Bearing Cave Deposits. Transvaal Museum Memoir doi:10.1016/j.mporth.2016.02.007.
- Brain, C.K., 1967. The Transvaal Museum's fossil project at Swartkrans'. S. Afr. J. Sci. 63, 378–384.
- Brain, C.K., 1976. A Re-interpretation of Swartkrans Site and it's remains. S. Afr. J. Sci. 72, 143–146.
- Brain, C.K., 1993. A taphonomic overview of the swartkrans fossil assemblages. In: Brain, C.K. (Ed.), Swartkrans: A Cave's Chronicle of Early Man. Transvaal Museum, Pretoria, pp. 257–264.
- Brain, C.K., 1995. The influence of climatic changes on the completeness of the early hominin record in southern African caves, with particular reference to swartkrans. In: Vrba, E.S. (Ed.), Palaeoclimate and Evolution, with Emphasis on Human Origins. New Haven 385e424.
- Bromage, T.G., Schrenk, F., Juwayeyi, Y.M., 1995. Paleobiogeography of the Malawi rift: age and vertebrate paleontology of the Chiwondo Beds, northern Malawi. J. Hum. Evol. 28, 37–57.
- Broom, R., 1925. Records of the Albany Museum. In: Records of the Albany Museum, 3. Grahamstown, pp. 307–308.
- Broom, R., 1936. New fossil anthropoid skull from South Africa. Nature 138, 486. doi:10.1038/138486a0.
- Broom, R., 1937. Discovery of a lower molar of Australopithecus. Nature 140, 681. doi:10.1038/140681a0.
- Broom, R., 1938. The Pleistocene anthropoid apes of South Africa. Nature 142, 377. doi:10.1038/142377a0.
- Broom, R., 1939. A preliminary account of the Pleistocene carnivores of the Transvaal caves. Ann. Transvaal Museum 331–338.
- Broom, R., Robinson, J.T., 1949. A new type of fossil man. Nature 164, 322-323.
- Bruxelles, L., Clarke, R.J., Maire, R., Ortega, R., Stratford, D., 2014. Stratigraphic analysis of the Sterkfontein StW 573 *Australopithecus* skeleton and implications for its age. J. Hum. Evol. 70 (1), 36–48. doi:10.1016/j.jhevol.2014.02.014.
- Bruxelles, L., Maire, R., Couzens, R., Thackeray, J.F., Braga, J., 2017. A revised stratigraphy of Kromdraai. In: Braga, Thackeray, F. (Eds.), Kromdraai, a Birthplace of Paranthropus in the Cradle of Humankind. Sun Media, pp. 31–47.
- Button, A., 1973. The stratigraphic history of the Malmani dolomite in the eastern and north-eastern Transvaal. Trans. Geol. Soc. South Afr. 76, 229–247.
- Butzer, K.W., 1976. Lithostratigraphy of Swartkrans formation. S. Afr. J. Sci. 72 (5), 136–141. Available atpapers3://publication/uuid/3B480A81-DCDB-450D-A48C-5E2202CB584F.
- Clarke, R.J., 1994. On some new interpretations of Sterkfontein stratigraphy. S. Afr. J. Sci. 90, 211-214.
- Clarke, R.J., 1998. South African journal of science. S. Afr. J. Sci.. Academy of Science for South Africa (ASSAf). Available at: https://journals.co.za/content/ sajsci/94/10/AJA00382353 236.
- Cooke, H.B.S., 1938. The Sterkfontein Bone Breccia: a Geological Note. S. Afr. J. Sci. 204–208.

- Cooke, H.B.S., 1991. Dinofelis barlowi (Mammalia, Carnivora, Felidae) cranial material from Bolt's Farm, collected by the University of California African expedition'. Palaeontol. Afr. 28, 9–21.
- Cooke, H.B.S., 1993. Undescribed suid remains from Bolt's farm and other Transvaal cave deposits. Palaeontol. Afr. 30, 7–23.
- Cooke, H.B.S., 2005. Stratigraphic variation in Suidae from the Shungura Formation and some coeval deposits. In: Bobe, R., Alemseged, Z., Behrensmeyer, A.K. (Eds.), Hominin Environments in the East African Pliocene: An Assessment of the Faunal Evidence, Vertebrate Paleobiology and Paleoanthropology Series. Springer, pp. 107–127.
- Dale, M.M., 1948. 'New fossil Suidae from Limeworks Quarry, Makapansgat, Potgietersrust. S. Afr. J. Sci. 2, 114–116.
- Dart, R.A., 1925. Australopithecus africanus: the man-Ape of South Africa. Nature 115, 504-508
- Dearing, J.A., Dann, R.J.L., Hay, K., Lees, J.A., Loveland, P.J., Maher, B.A., O'Grady, K., 1996. Frequency-dependent susceptibility measurements of environmental materials. Geophys. J. Int. 124, 228–240.
- Deino, A.L., 2012. '40Ar/39Ar dating of Bed 1, Olduvai Gorge, Tanzania, and the chronology of early Pleistocene climate change. J. Hum. Evol. 63, 251–273.
- De Ruiter, D.J., Berger, L.R., 2000. Leopards as taphonomic agents in dolomitic cavesimplications for bone accumulations in the hominid-bearing deposits of South Africa. J. Archaeol. Sci. 27 (8), 665–684. doi:10.1006/jasc.1999.0470.
- Dirks, P.H.G.M., Kibii, J.M., Kuhn, B.F., Steininger, C., Churchill, S.E., Kramers, J.D., Pickering, R., Farber, D.L., Mériaux, A.S., Herries, A.I.R., King, G.C.P., Berger, L.R., 2010. Geological setting and age of *Australopithecus sediba* from southern Africa. Science 328 (5975), 205–208. doi:10.1126/science.1184950.
- Dirks, P.G.H.M., Roberts, E.M., Hilbert-Wolf, H., Kramers, J.D., Hawks, J., Dosseto, A., Duval, M., Elliott, M., Evans, M., Grün, R., Hellstrom, J., Herries, A.I.R., Joannes-Boyau, R., Makhubela, T.V., Placzek, C.J., Robbins, J., Spandler, C., Wiersma, J., Woodhead, J., Berger, L.R., 2017. The age of *Homo naledi* and associated sediments in the Rising Star Cave, South Africa. Elife 6, 1–59. doi:10.7554/elife.24231.
- Dirks, P.H.G.M., Berger, L.R., 2013. Hominin-bearing caves and landscape dynamics in the Cradle of Humankind, South Africa. J. Afr. Earth Sci. 78, 109–131. doi:10.1016/j.jafrearsci.2012.09.012.
- Edwards, T.R., Grono, E., Herries, A.I.R., Brink, F.J., Troitzsch, U., Senden, T., Turner, M., Barron, A., Prossor, L., Denham, T., 2017. Visualising scales of process: multi-scalar geoarchaeological investigations of microstratigraphy and diagenesis at hominin bearing sites in South African karst. J. Archaeol. Sci. 83, 1–11. doi:10.1016/j.jas.2017.05.007, Elsevier Ltd.
- Edwards, T.R., Birkett-Rees, J., Herries, A.I.R., Blackwood, A.F., Adams, J.W., Armstrong, B.J., Pickering, R., Penzo-Kajewski, P., 2019. Combining legacy data with new drone and DGPS mapping to identify the provenance of Plio-Pleistocene fossils from Bolt's Farm, Cradle of Humankind (South Africa). PeerJ 7, e6202. doi:10.7717/peerj.6202.
- Eriksson, K.A., Truswell, J.F., 1975. A palaeoenvironmental interpretation of the early Proterozoic Malmani dolomite from Zwartkops, South Africa. Precambrian Res. 2 (3), 277–303. doi:10.1016/0301-9268(75)90013-3.
- Eriksson, P.G., Schweitzer, J.K., Bosch, P.J.A., Schereiber, U.M., Van Deventer, J.L., Hatton, C.J., 1993. The transvaal sequence: an overview. J. Afr. Earth Sci. 16 (1–2), 25–51. doi:10.1016/0899-5362(93)90160-R.
- Ewer, R.F., 1958. The fossil Suidae of Makapansgat. Proc. Zool. Soc. Lond. 130, 329–372.
  Fiore, I., Tagliacozze, A., 2004. Taphonomic analysis of the bone remains from the Oldowan site of Garba IV. In: Chavailion, J., Piperno, M (Eds.), Studies On the Early Paleolithic Site of Melka Kunture, Ethiopia. Istituto Italiano di Preistoria e Protoistoria, pp. 639–682.
- Fisher, R., 1953. Dispersion on a sphere, 217, pp. 295-305.
- Fourvel, J.B., 2018. Civettictis braini nov. sp. (Mammalia:carnavora), a new viverrid from the hominin-bearing site of Kromdraai (Gauteng, South Africa). Comptes Rendus Palevol 17 (6), 366–377.
- Fourvel, J.B., Brink, J., Beaudet, A., Pavia, M., 2016. Some preliminary interpretations of the oldest faunal assemblages from Kromdraai. In: Braga, J., Thackeray, F. (Eds.), Kromdraai: a Birthplace of Paranthropus in the Cradle of Humankind. Sun Press, Johannesburg, pp. 71–106.
- Freedman, L., 1957. The fossil Cercopithecoidea of South Africa. Ann. Transvaal Museum 23, 121–261
- Gentry, A., 2010. Bovidae. In: Werdelin, L., L., Sanders, W (Eds.), Cenozoic Mammals of Africa. Univ. California Press, pp. 741–796.
- Geraads, D., Eisenmann, V., Petter, G., 2004. The Large Mammal Fauna of the Oldowayan sites of Melka-Kunturé, Ethiopia. In: Chavailion, J., Piperno, M (Eds.), Studies On the Early Paleolithic Site of Melka Kunture. Istituto Italiano di Preistoria e Protoistoria, Ethiopia, pp. 169–192.
- Gommery, D., Thackeray, J.F., Sénégas, F., Potze, S., Kgasi, L., 2008. The earliest primate (*Parapapio sp.*) from the Cradle of Humankind World Heritage site (Waypoint 160, Bolt's Farm, South Africa). S. Afr. J. Sci. 104 (9–10), 405–408.
- Gommery, D., Sénégas, F., Kgasi, L., Vilakazi, N., Kuhn, B., Brink, J., Pickford, M., Herries, A.I.R., Hancox, J., Saos, T., Ségalen, L., Julie Aufort, J., Thackeray, F.J., 2016. 'Bolt's Farm Cave System in the Cradle of Humankind (South Africa): an example of multidisciplinary approach to the study of fossil primate sites'. Revue de Primatologie 7, 24.
- Granger, D.E., Gibbon, R.J., Kuman, K., Clarke, R.J., Bruxelles, L., Caffee, M.W., 2015. New cosmogenic burial ages for Sterkfontein Member 2 Australopithecus and Member 5 Oldowan. Nature 522 (7554), 85–88. doi:10.1038/nature14268.
- Haughton, S.H., 1947. Notes on the Australopithecine-bearing rocks of the Union of South Africa, Trans. Geol. Soc. South Afr. 55 (371), 55–59.
- Harris, J.M., White, T.D., 1979. Evolution of the Plio-Pleistocene African Suidae. Trans. Am. Philos. Soc. 69 (2), 1–128.

- Harris, J.M., 1991. Family Bovidae. In: Harris, JM (Ed.), Koobi Fora Research Project, Vol 3. Clarendon Press, Oxford, pp. 139–320 editor.
- Herries, A.I.R., Reed, K.E., Kuykendall, K.L., Latham, A.G., 2006. Speleology and magnetobiostratigraphic chronology of the Buffalo Cave fossil site, Makapansgat, South Africa. Quat. Res. 66 (2), 233–245. doi:10.1016/j.yqres.2006.03.006.
- Herries, A.I.R., Curnoe, D., Adams, J.W., 2009. 'A multi-disciplinary seriation of early Homo and Paranthropus bearing palaeocaves in southern Africa'. Quat. Int. 202 (1–2), 14–28.
- Herries, A.I.R., Pickering, R., Adams, J.W., Curnoe, D., Warr, G., Latham, A.G., Shaw, J., 2013. A multi-disciplinary perspective on the age of Australopithecus in Southern Africa. In: Reed, K.E., Fleagle, J.G., Leakey, R.E. (Eds.), The Paleobiology of Australopithecus. Springer, DordrechtNetherlands, pp. 21–40. doi:10.1007/978-94-007-5919-0\_3.
- Herries, A.I.R., Kappen, P., Kegley, A.D.T., Patterson, D., Howard, D.L., De Jonge, M.D., Potze, S., Adams, J.W., 2014. Palaeomagnetic and synchrotron analysis of > 1.96 Ma fossil-bearing palaeokarst ay Haasgat, South Africa. S. Afr. J. Sci. 110 (3–4), 1–12. doi:10.1590/sais.2014/20130102.
- Herries, A.I.R., Murszewski, A., Pickering, R., Mallett, T., Joannes-Boyau, R., Armstrong, B., Adams, J.W., Baker, S., Blackwood, A.F., Penzo-Kajewski, P., Kappen, P., Leece, A.B., Martin, J., Rovinsky, D., Boschian, G., 2018. Geoarchaeological and 3D visualisation approaches for contextualising in-situ fossil bearing palaeokarst in South Africa: a case study from the ~2.61 Ma Drimolen Makondo. Quat. Int. 483, 90–110. doi:10.1016/j.quaint.2018.01.001.
- Herries, A.I.R., Martin, J.M., Leece, A.B., Adams, J.W., Boschian, G., Joannes-Boyau, R., Edwards, T.R., Mallett, T., Massey, J., Murszewski, A., Neubauer, S., Pickering, R., Strait, D., Armstrong, B.J., Baker, S., Caruana, M.V., Denham, T., Hellstrom, J., Moggi-Cecchi, J., Mokobane, S., Penzo-Kajewski, P., Rovinsky, D.S., Schwartz, G.T., Stammers, R.C., Wilson, C., Woodhead, J., Menter, C., 2020. Contemporaneity of Australopithecus, Paranthropus and early Homo erectus in South Africa. Science 368 (6486). doi:10.1126/science.aaw7293.
- Herries, A.I.R., Shaw, J., 2011. Palaeomagnetic analysis of the Sterkfontein palaeocave deposits: implications for the age of the hominin fossils and stone tool industries. J. Hum. Evol. 60 (5), 523–539. doi:10.1016/j.jhevol.2010.09.001.
- Heslop, D., Roberts, A.P., 2016. Analyzing paleomagnetic data: to anchor or not to anchor?
  J. Geophys. Res.: Solid Earth 121 (11), 7742–7753. doi:10.1002/2016JB013387.
- Hopley, P.J., Marshall, J.D., Weedon, G.P., Latham, A.G., Herries, A.I.R., Kuykendall, K.L., 2007. Orbital forcing and the spread of C 4 grasses in the late Neogene: stable isotope evidence from South African speleothems. J. Hum. Evol. 53, 620–634. doi:10.1016/j.jhevol.2007.03.007.
- Hopley, P., Herries, A.I.R., Baker, S., Kuhn, B., Menter, C., 2013. Beyond the South African Cave Paradigm - Australopithecus Africanus from the Pliocene palaeosol deposits of Taung. Am. J. Phys. Anthropol. 151, 316–324.
- Ingram, B.A., Van Tonder, D.M., 2011. The Geology of the Broederstroom Area. Council for Geosceince, South Africa.
- Jarvis A., Reuter H.I., Nelson A., Guevera E., 2008. Hole-filled SRTM for the globe. Version 4. Available at http://srtm.csi.cgiar.org.
- Keyser, A.W., Menter, C.G., Moggi-Cecchi, J., Pickering, T.R., Berger, L.R., 2000. Drimolen: a new hominid-bearing site in Gauteng, South Africa.. S. Afr. J. Sci. 96, 102, 107
- Kidane, T., Brown, F.H., Kidney, C., 2014. Magnetostratigraphy of the Fossil-Rich Shungura formation, southwest, Ethiopia. J. Afr. Earth Sci. 97, 207–223.
- King, L., 1951. The geology of the Makapan and other caves. Trans. R. Soc. South Afr. 33 (1), 121–151.
- Kirschvink, J.L., 1980. The least-squares line and plane and the analysis of palaeomagnetic data. Geophys. J. 699–718.
- Kramers, J.D., Dirks, P.H.G.M., 2017. The age of fossil StW573 ('Little Foot'): an alternative interpretation of 26Al/10Be burial data'. S. Afr. J. Sci. 113 (3–4), 1–8. doi:10.17159/sajs.2017/20160085.
- Kos, A.M., 2001. Stratigraphy, sedimentary development and palaeoenvironmental context of a naturally accumulated pitfall cave deposit from southeastern Australia. Austr. J. Earth Sci. 48, 621–632. doi:10.1046/j.1440-095.2001.485885.x.
- Lacruz, R.S., Brink, J.S., Hancox, P.J., Skinner, A.S., Herries, A., Schmid, P., Berger, L.R.., 2002. 'Palaeontology and geological context of a middle Pleistocene Faunal Assemblage from the Gladysvale Cave, South Africa'. Palaeontol. Africana 38, 99-114.
- Latham, A.G., Herries, A.I.R., Quinney, P., Sinclair, A., Kuykendall, K., 1999. The Makapansgat Australopithecine Site from a Speleological Perspective. In: The Makapansgat Australopithecine Site from a Speleological Perspective, 165. Geological Society, London, Special Publications, pp. 61–77. doi:10.1144/gsl.sp.1999.165.01.05.
- Latham, A.G., Herries, A.I.R., Sinclair, A.G.M., Kuykendall, K., 2002. Re-examination of the lower stratigraphy of the classic section, limeworks site, Makapansgat, South Africa. Hum. Evol. 17 (3–4), 207–214. doi:10.1007/BF02436372.
- Latham, A.G., Herries, A.I., Kuykendall, K., 2003. The formation and sedimentary infilling of the Limeworks Cave, Makapansgat, South Africa'. Palaeontol. Afr. 39, 69–82.
- Lazagabaster, I.A., Souron, A., Rowan, J., Robinson, J.R., Campisano, C.J., Reed, K.E., 2018a. a. Fossil Suidae (Mammalia, Artiodactyla) from Lee Adoyta, Ledi-Geraru, lower Awash Valley, Ethiopia: implications for the late Pliocene turnover and paleoecology. Palaeogeogr. Palaeoclimatol. Palaeoecol. 504, 186–200.
- Lazagabaster, I.A., Brophy, J., Sanisidro, O., Pineda-Munoz, S., Berger, L., 2018b. A new partial cranium of *Metridiochoerus* (Suidae, Mammalia) from Malapa, South Africa. J. Afr. Earth Sci. 145, 49–52.
- Leakey, L.S.B., 1943. New fossil Suidae from Shungura. Omo J . E. Afr. nut. Hwt. Soc. 17, 45–61.
- Lee-Thorp, J.A., Talma, A.S., 2000. Stable light isotopes and environments in the Southern African Quaternary and Late Pliocene. In: Partridge, T.C., Maud, R.R. (Eds.), The Cenozoic of Southern Africa. Oxford Monographs on Geology and Geophysics. Oxford University Press, Oxford, p. 236e251.

- Leonhardt, R., 2006. Analyzing rock magnetic measurements: the RockMagAnalyzer 1 . 0 software. Comput. Geosci. 32, 1420–1431. doi:10.1016/j.cageo.2006.01.006.
- Ludwig, K.R., 2000. Decay constant errors in U Pb concordia-intercept ages. Chem. Geol. 166, 315–318 doi: 0009-254-00.
- Martini, J.E., Wipplinger, P.E., Moen, H.F., Keyser, A., 2003. Contribution to the speleology of Sterkfontein cave, Gauteng Province, South Africa. Int. J. Speleol. 32 (1), 135–144.
- Maxbauer, D.P., Feinberg, J.M., Fox, D.L., 2016. Computers & Geosciences MAX UnMix: a web application for unmixing magnetic coercivity distributions. Comput. Geosci. 95, 140–145. doi:10.1016/j.cageo.2016.07.009.
- McFadden, P.L., Brock, A., Partridge, T.C., 1979. Palaeomagnetism and the age of the Makapansgat hominid site. Earth Planet. Sci. Lett. 44, 373–382.
- Miall, A., 2014. Fluvial Depositional Systems. Springer Geology doi:10.1007/978-3-319-00666-6.
- Moriarty, K.C, et al., 2000. Mid-Pleistocene cave fills, megafaunal remains and climate change at Naracoorte, South Australia: towards a predictive model using U-Th dating of speleothems. Palaeogeogr. Palaeoclimatol. Palaeoecol. 159 (1–2), 113–143. doi:10.1016/S0031-0182(00)00036-5.
- McKee, J.K., 1993. Faunal dating of the Taung hominid fossil deposit. J. Hum. Evol. 25, 363–376
- Monson, T.A., Brasil, M.F., Hlusko, L.J., 2015. Material collected by the southern branch of the UC Africa Expedition with a report on previously unpublished Plio-Pleistocene fossil localities. PaleoBios 32 (1), 1–17.
- Moskowitz, B.M., 1981. Methods for estimating Curie temperatures of titanomaghemites from experimental Js-T data. In: Earth and Planetary Science Letters, 53. Elsevier, pp. 84–88. doi:10.1016/0012-821X(81)90028-5.
- Obbes, A.M., 2000. The Structure, Stratigraphy and Sedimentology of the Black Reef-Malmani-Rooihoogte Succession of the Transvaal Supergroup Southwest of Pretoria. The Structure, Stratigraphy and Sedimentology of the Black Reef-Malmani-Rooihoogte Succession of the Transvaal Supergroup Southwest of Pretoria, 127. Council for Geoscience South Africa Bulletin.
- Partridge, T.C., 1978. Re-appraisal of lithostratigraphy of Sterkfontein hominid site. Nature 275 (5678), 282–287. doi:10.1038/275282a0.
- Partridge, T.C., 1979. Re-appraisal of lithostratigraphy of Makapansgat Limeworks hominid site. Nature 279 (5713), 484–488. doi:10.1038/279484a0.
- Partridge, T.C., 2000. Hominid-bearing cave and tufa deposits. Oxford Monogr. Geol. Geophys. 40, 100–130.
- Partridge, T.C., Granger, D.E., Caffee, M.W., Clarke, R.J., 2003. Lower Pliocene Hominid Remains from Sterkfontein. Science 300, 607–612.
- Petrovský, E. and Kapiĉka, A. (2006) 'On determination of the Curie point from thermomagnetic curves', 111, pp. 1–10. doi: 10.1029/2006JB004507.
- Pickford, M., 2013. 'Locomotion, diet, body weight, origin and geochronology of Metridiochoerus andrewsi from the Gondolin Karst Deposits, Hauteng, South Africa'. Ann. Ditsong Natl. Mus. Nat. Hist. 3 (1), 33–47.
- Pickford, M., Gommery, D., 2016. Fossil Suidae (Artiodactyla, Mammalia) from Aves Cave I and nearby sites in Bolt's Farm Palaeokarst System, South Africa'. Estudios Geologicos-Madrid 72 (2). doi:10.3989/egeol.42389.404.
- Pickford, M., Gommery, D., 2020. Fossil suids from Bolt's farm Palaeokarst system, South Africa implications for the taxonomy of *Potamochoeroides* and *Notochoerus* and for biochronology. Estudios Geológicos 76 (1), e127.
- Pickford, M., Gommery, D., Kgasi, L., Vilakazi, N., Senut, B., Mocke, H., 2019. Southern African Tetraconodontinae: recent discoveries. Commun. Geol. Surv. Namibia 21, 59–81.
- Pickering, R., Hancox, P.J., Lee-Thorp, J.A., Grün, R., Mortimer, G.E., McCulloch, M., Berger, L.R., 2007. Stratigraphy, U-Th chronology, and paleoenvironments at Gladysvale Cave: insights into the climatic control of South African hominin-bearing cave deposits. J. Hum. Evol. 53 (5), 602–619. doi:10.1016/j.jhevol.2007.02.005.
- Pickering, R., Kramers, J.D., Partridge, T., Kodolanyi, J., Pettke, T., 2010a. U Pb dating of calcite – aragonite layers in speleothems from hominin sites in South Africa by MC-ICP-MS. Quat. Geochronol. 5 (5), 544–558. doi:10.1016/j.quageo.2009.12.004, Elsevier B.V.
- Pickering, R., Dirks, P.H.G.M., Jinnah, Z., De Ruiter, D.J., Churchil, S.E., Herries, A.I.R., Woodhead, J.D., Hellstrom, J.C., Berger, L.R., 2011a. and Implications for the Origins of the Genus *Homo*. Science 333, 1421–1423.
- Pickering, R., Kramers, J.D., Hancox, P.J., De Ruiter, D.J., Woodhead, J.D., 2011. Contemporary flowstone development links early hominin bearing cave deposits in South Africa. Earth Planet. Sci. Lett. 306 (1–2), 23–32. doi:10.1016/j.epsl.2011.03.019.
- Pickering, R., Kramers, J.D., Partridge, T., Kodolanyi, J., Pettke, T., 2010b. Pb dating of calcite – aragonite layers in speleothems from hominin sites in South Africa by MC-ICP-MS. Quat. Geochronol. 5 (5), 544–558. doi:10.1016/j.quageo.2009.12.004, Elsevier B.V.
- Pickering, R., Herries, A.I.R., Woodhead, J.D., Hellstrom, J.C., Green, H.E., Paul, B., Ritzman, T., Strait, D.S., Schoville, B.J., Hancox, P.J., 2019. U-Pb-dated flowstones restrict South African early hominin record to dry climate phases. Nature 565 (7738), 226–229. doi:10.1038/s41586-018-0711-0.

- Pickering, R., Herries, A.I.R., 2020. New multi-disciplinary age estimates for the Sterk-fontein Member 4 australopithecines. In: Ward, C., Richmond, B., Zipfel, B. (Eds.), Hominin Postcranial Remains from Sterkfontein Eds. Oxford University Press, South Africa. Oxford.
- Rannikko, J., Žliobaitėa, I., Fortelius, M., 2017. Relative abundances and palaeoecology of four suid genera in the Turkana Basin, Kenya, during the late Miocene to Pleistocene. Palaeogeogr. Palaeoclimatol. Palaeoecol. 487, 187–193.
- Reynolds, S.C., Kibii, J.M., 2011. Sterkfontein at 75: review of palaeoenvironments, fauna and archaeology from the hominin site of Sterkfontein (Gauteng Province, South Africa). Palaeontol. Afr. 46. 59–88.
- Roberts, D.M., T., Herries, A.I.R, Boulter, C., Scott, L., Dondo, C., Mtembi, P., Browning, C., Smith, R., Haarhoff, 2011. 'Regional and global palaeoenvironmental and sea level context of the late cenozoic langebaanweg (LBW) palaeontological site: west coast of South Africa. Earth-Sci. Rev. 106, 191–214.
- Rovinsky, D.S., Herries, A.I.R., Menter, C.G., Adams, J.W., 2015. First description of in situ primate and faunal remains from the Plio-Pleistocene Drimolen Makondo palaeocave infill, Gauteng, South Africa'. Palaeontol. Electron. June, 1–21. doi:10.26879/533.
- Senegas, F., Avery, M., 1998. New Evidence for the Murine Origins of the Otomyinae (Mammalia, Rodentia) and the age of Bolt's Farm (South Africa)'. S. Afr. J. Sci. 94, 503–507.
- South African Committee for Stratigraphy (SACS), 1980. 'Part 1: lithostratigraphy of the Republic of South Africa, South West Africa/Namibia and the Republics of Bophuthatswana. Transkei and Venda', Stratigraphy of South Africa. Government Printer. South Africa.
- Sponheimer, M., Reed, K.E., Lee-Thorp, J.A., 1999. Combining isotopic and ecomorphological data to refine bovid paleodietary reconstruction: a case study from the Makapansgat Limeworks hominin locality. J. Hum. Evol. 36 (6), 705–718. doi:10.1006/jhev.1999.0300.
- Stammers, R.C., Caruana, M.V., Herries, A.I.R., 2018. The first bone tools from Kromdraai and stone tools from Drimolen, and the place of bone tools in the South African Earlier Stone Age. Quat. Int. 495 (September 2017), 87–101. doi:10.1016/j.quaint.2018.04.026.
- Stratford, D., Grab, S., Pickering, T.R., 2014. The stratigraphy and formation history of fossil- and artefact-bearing sediments in the Milner Hall, Sterkfontein Cave, South Africa: new interpretations and implications for palaeoanthropology and archaeology. J. Afr. Earth Sci. 96, 155–167. doi:10.1016/j.jafrearsci.2014.04.002.
- Susman, R.L., 1988. New postcranial remains from Swartkrans and their bearing on the functional mor-phology and behavior of *Paranthropus robustus*. In: Grine, F.E. (Ed.), The Evolutionary History of the "Robust" Australopithecines. Aldine de Gruyter, New York, pp. 149–172.
- Susman, R.L., 1989. New hominid fossils from the Swartkrans Formation (1979–1986 excavations), postcranial specimens. Am. J. Phys. Anthropol. 79, 451–474.
- Suwa, G., Nakaya, H., Asfaw, B., Saegusa, H., Amzaye, A., Kono, R.T., Beyene, Y., Katoh, S., 2003. Plio-Pleistocene terrestrial mammal assemblage from Konso, southern Ethiopia. J. Vertebr. Paleontol. 23, 901–916.
- Tauxe, L., Mullender, T.A.T., Pick, T., 1996. Potbellies, wasp-waists, and superparamagnetism in magnetic hysteresis. J. Geophys. Res.: Solid Earth 101 (B1), 571–583. doi:10.1029/95ib03041.
- Thackeray, J.F., Kirschvink, J.L., Raub, T.D., 2002. Palaeomagnetic analyses of calcified deposits from the Plio-Pleistocene hominid site of Kromdraai, South Africa. S. Afr. J. Sci. 98, 537–540.
- Van der Merwe, N.J., Thackeray, J.F., 1997. 'Stable carbon isotope analysis of Plio-Pleistocene ungulate teeth from Sterkfontein, South Africa. S. Afr. J. Sci. 93, 194.
- Vrba, E.S., 1995. The fossil record of African antelopes (Mammalia, Bovidae) in relation to human evolution and paleoclimate. In: Vrba, E.S, Denton, G.H., Partridge, T.C., Burckle, L.H (Eds.), Palaeoclimate and Evolution with Emphasis On Human Origins. Yale University Press, pp. 385–424.
- Walden, J., 1999. Environmental magnetism: a practical guide. In: Oldfield, F., Smith, J. (Eds.), Tech. Guide 6. Quaternary Research Association, London.
- Werdelin, L., Peigné, S., 2010. Carnivora. In: Werdelin, L., Sanders, W.J. (Eds.), The Cenezoic Mammals of Africa. University of California Press, pp. 603–658.
- White, W.B., 2007. Cave sediments and paleoclimate. J. Cave Karst Stud. 69 (1), 76–93. doi:10.1103/physrev.2.109.
- White, T.D., Clark Howell, F., Gilbert, H., 2006. The earliest Metridiochoerus (Artiodactyla: suidae) from the Usno Formation, Ethiopia. Trans. R. Soc. South Afr. 61 (2,), 75–79.Wilkinson, M.J., 1973. Sterkfontein Cave System: Evolution of a Karst Form Unpublished
- M.A thesis. University of the Witswatersrand.Wilkinson, M.J., 1983. 'Geomorphic perspectives on the Sterkfontein australopithecine
- breccias. J. Archaeol. Sci. 10, 515–529.
  Woodhead, J., Hellstrom, J., Maas, R., Drysdale, R., Zanchetta, G., Devine, P., Taylor, E., 2006. U Pb geochronology of speleothems by MC-ICPMS. Quat. Geochronol. 1, 208–221. doi:10.1016/j.quageo.2006.08.002.
- Wood, B.K., Boyle, E., 2016. Hominin taxic diversity: fact or fantasy? Am. J. Phys. Anthropol. 159, S37–S78. doi:10.1002/ajpa.22902.